Elsevier Editorial System(tm) for Continental Shelf Research

Manuscript Draft

Manuscript Number:

Title: Hydrodynamics in the Gulf of Aigues-Mortes, NW Mediterranean Sea: in situ and modelling data

Article Type: Research Paper

Section/Category:

Keywords: current data; modelling; shelf dynamics; wind-induced currents

Corresponding Author: Dr. Leredde Yann, PhD

Corresponding Author's Institution: Université Montpellier 2

First Author: Leredde Yann, PhD

Order of Authors: Leredde Yann, PhD; Denamiel Cléa, DEA; Bouchette Frédéric, PhD; Lauer-Leredde Christine, PhD; Marsaleix Patrick, PhD

Manuscript Region of Origin:

Abstract: The Gulf of Aigues-Mortes (NW Med. Sea) is an inner shelf zone which scale is an intermediate between the nearshore and the coastal scales. Its hydrodynamics is for the first time investigated. ADCP, CTD and thermosalinograph data were collected during three short cruises (HYGAM; March 6-7, 20-21, April 5-6, 2005). They were scheduled approximately every 15 days to sample the gulf circulation under different weather conditions but also to be included as data of validation of a single numerical modelling. Circulation features displayed by in situ data are well reproduced by Symphonie, a 3D circulation model based on Boussinesq and hydrostatic approximations. A downscaling modelling approach is implemented, the largest scale being obtained by the replay of the MFSTEP regional model of the North Western Mediterranean Sea.

The analysis, closely coupling in situ measurements and model results, provides information that would not have been obtained using data separately. The great variability of the oceanic circulation at this scale is well evidenced. Winds are the main forcing, locally, but also at a larger scale. North winds generate consistent structures interacting with the general Mediterranean circulation. The explanation of the induced currents is then not straightforward, some of them being for example northward. South and southeast winds reinforce the slopping surface, this latter allowing the geostrophic equilibrium with longshore currents. These winds can also generate swells indirectly influencing the circulation. This study, focused on the end of winter 2004-2005, also enhances the thermic exchanges from offshore to nearshore, as well as the initiation of shelf dense waters.

Manuscript
Click here to download Manuscript: leredde0706.doc

Hydrodynamics in the Gulf of Aigues-Mortes, NW Mediterranean Sea: *in situ* and modelling data

Yann LEREDDE [(1)*], Cléa DENAMIEL [(1)], Frédéric BOUCHETTE [(1)], Christine LAUER-LEREDDE [(1)], Patrick MARSALEIX [(2)]

(1) Laboratoire Dynamique de la Lithosphère - UMR CNRS-UM2 5573. Université Montpellier 2. CC. 60, place E. Bataillon. 34095 Montpellier cedex 5. France.

(2) Laboratoire d'Aérologie, UMR 5560 UPS-CNRS. Pôle d'Océanographie Côtière. 14, Avenue Edouard Belin. 31400 Toulouse. France.

* corresponding author. Tel.: + 33467143630; fax: + 33467143642. E-mail address: leredde@dstu.univ-montp2.fr

Abstract

The Gulf of Aigues-Mortes (NW Med. Sea) is an inner shelf zone which scale is an intermediate between the nearshore and the coastal scales. Its hydrodynamics is for the first time investigated. ADCP, CTD and thermosalinograph data were collected during three short cruises (HYGAM; March 6-7, 20-21, April 5-6, 2005). They were scheduled approximately every 15 days to sample the gulf circulation under different weather conditions but also to be included as data of validation of a single numerical modelling. Circulation features displayed by in situ data are well reproduced by *Symphonie*, a 3D circulation model based on Boussinesq and hydrostatic approximations. A downscaling modelling approach is implemented, the largest scale being obtained by the replay of the MFSTEP regional model of the North Western Mediterranean Sea.

The analysis, closely coupling *in situ* measurements and model results, provides information that would not have been obtained using data separately. The great variability of the oceanic circulation at this scale is well evidenced. Winds are the main forcing, locally, but

also at a larger scale. North winds generate consistent structures interacting with the general Mediterranean circulation. The explanation of the induced currents is then not straightforward, some of them being for example northward. South and southeast winds reinforce the slopping surface, this latter allowing the geostrophic equilibrium with longshore currents. These winds can also generate swells indirectly influencing the circulation. This study, focused on the end of winter 2004-2005, also enhances the thermic exchanges from offshore to nearshore, as well as the initiation of shelf dense waters.

Subject keywords current data, modelling, shelf dynamics, wind-induced currents

Regional index terms France, Western Mediterranean Sea, Gulf of Lions, Gulf of Aigues-Mortes, Languedoc-Roussillon region.

1. Introduction

The Gulf of Aigues-Mortes (GAM) is located in the Northwestern Mediterranean Sea (Fig. 1). This zone is the northern part of the Gulf of Lion inner shelf. It is also the shelf zone the most further off the continental slope, and so off the general Mediterranean circulation, i.e. the Northern Current (e.g. Millot, 1990). This zone is however largely open to offshore and can not be studied without taking into account the hydrodynamic and meteorological phenomena at large scale. Down to the 80 m-isobath, the slope is low, on the order of 0.5%. Beyond, the shelf is nearly flat, and this, until the shelf break. Except the harbour structures, the coast is sandy, and globally in erosion (e.g. Certain *et al*, 2005b and included literature). Urbanisation and tourism are intensively developed. The Montpellier area (Fig. 2) represents 400 000 habitants. The Sète harbour (Fig. 2) is the first French Mediterranean fishing port with roughly 15 000 T/yr of fish (tuna, sardine, anchovy, whiting, …). Port-Camargue (Fig. 2) is the first French Mediterranean yachting harbour with 4800 pier places. Numerous resorts, Palavas-les-Flots and La Grande Motte (Fig. 2) for example, extended very rapidly in the 60s, with the mass tourism development. The stakes are so crucial and scientific studies such as this one are expected by society and authorities.

At the GAM scale, the hydrodynamics is mainly induced by winds. Other forcings, like the Earth revolution (Coriolis effect) or the pressure and density gradients, should also be considered. As shown by Denamiel *et al* (2005), the waves induced currents can not be neglected. Previous studies do not allow to well understand the GAM hydrodynamics.

On the one hand, previous research studies focussed on the coastal oceanic circulation, and we should rather say, on the regional circulation. As far as the NW Mediterranean Sea is concerned, studies were indeed often centred on the whole Gulf of Lion (Fig. 1). For many years, the French National Program of Coastal Environment (Raimbault and Durrieu de Madron, 2000) has focussed on studies at regional scales. Experimental studies were carried out in the 90s in the region, especially on the variation of the Northern Current offshore of Marseilles (Conan & Millot, 1995), the sediment transport in canyons (Monaco *et al*, 1990) or at the shelf break (Durrieu de Madron *et al*, 1999; Lapouyade & Durrieu de Madron, 2001), the biogeochemical cycles in the gulf (Raimbault and Durrieu de Madron, 2000), and the Rhone River plume (Naudin *et al*, 2001; and included literature). More recently the entire shelf circulation has been studied (Petrenko *et al*, 2005) and the interactions with the general Mediterranean circulation is the main point that will be studied in the next years. Previous modelling works focussing on Gulf of Lion dynamics have been done with primitive equations models based on Boussinesq and hydrostatic approximation, using either cartesian coordinates and rigid lid (Delleville, 1997; Echevin *et al*, 2003) or sigma coordinates and free surface (Estournel *et al*, 2003) formalism.

On the other hand, other studies are very close to the coast, describing the evolution of a single beach considering swell dynamics only, and more particularly surf effects, ignoring low frequency meso-scale patterns. As far as our location site is concerned, the Sète beach (Fig. 2) was previously studied thanks to observations (Tessier *et al*, 2000; Certain *et al*, 2005a) or numerical experiments (Meulé *et al*, 2001). These nearshore scale studies are totally disconnected from the previous regional scale studies. Both observations and modelling tools are very different.

At the intermediate scale, hydrodynamics have been very poorly studied. Except a few studies, such as the Gulf of Fos ones (Ulses *et al*, 2005), no study looked particularly at the hydrodynamics of the NW Mediterranean littoral. It is however essential to understand the hydrodynamics at this intermediate scale if we want to understand the biogeochemical and sedimentary exchanges between the coast and the high sea.

The GAM hydrodynamics is then still not well known and the aim of this paper is to give first clues. The main objectives of the paper are to test whether the hydrodynamic features observed quasi-synoptically throughout the whole GAM can be reproduced by a 3D circulation model. We will show that the model can be used to better understand the generating processes of the observed currents in a lot of cases. We will also see that some effects such as those induced by swells, ignored in this numerical study, are likely to explain some of the model's failures.

Both the Methods section (Section 2) and the Results section (Section 3) present first the data and second the model or its outputs. In the final section, the main results are summarized, and some perspective work, briefly described.

2. Methods

2.1. The HYGAM cruises

Three short cruises (HYGAM: HYdrodynamics in the Gulf of Aigues-Mortes) were done in March-April 2005 to survey hydrodynamics features across the GAM. They were scheduled approximately every 15 days to sample the gulf circulation under different weather conditions but also to be included as data of validation of a single numerical modelling. The cruises took place during March 6-7, 20-21 and April 5-6, 2005, leaving from and returning to Sète, France (Fig. 2). In order to get a quasi-synoptic view of the circulation, the RV Téthys II covered the entire gulf as quickly as possible with, as an upper speed limit, the speed above which data acquisition quality would be altered (8 knots). With these conditions, the entire gulf was covered quickly performing regular CTD stations. Otherwise, throughout the cruise, continuous measurements were made with a RD Instruments hull-mounted ADCP, a Seabird thermosalinograph connected to a pumping system and a Batos meteorological station.

The ADCP is a broadband VMBB 150 kHz. The configuration used during all cruises is identical: 60 cells, 4 m depth bins, an ensemble average of 1 minute, and bottom tracking when possible. Precision on the ADCP data is better than 0.02 m s^{-1}. Thermosalinograph and CTD data were analyzed with the Seasoft software (http://www.seabird.com/software/Seasoft.htm).

Wind was measured every 15 s by the meteorological station Batos, on board the ship. These data were averaged every 30 mn. Moreover, the coastal weather station data of Sète, La Grande-Motte and Port-Camargue (see locations on Fig. 2), were gently provided by Météo-France. Both for analysis and modelling, the meteorological conditions need also to be known before the cruise (not only during the cruise) and throughout the Northwestern Mediterranean sea (not only on the cruise track). Hence, Aladin, a weather-forecast model, was used to provide the necessary additional meteorological information. Winds modelled by Aladin are averaged over a 3-hours period, on a 0.1°-0.1° grid throughout the gulf.

2.2. The circulation model

In this paper, modelling is carried out with the *Symphonie* model, which description can be found in Ulses *et al* (2005), Pairaud and Auclair *et al* (2003), Petrenko *et al* (2005), Estournel *et al* (2005), together with recent examples of applications. This model belongs to the family of models based on Boussinesq and hydrostatics approximations, using a sigma coordinate formalism and having a free surface elevation, as the well known POM (Blumberg and Mellor, 1987) and ROMS (Shchepetkin and McWilliams, 2005) models. The three components of the current, surface elevation, temperature and salinity are computed on a C grid, using classical finite difference methods. The turbulence closure is achieved through a prognostic equation for the turbulent kinetic energy and a diagnostic equation for the mixing and dissipation length scales (Gaspar *et al*, 1990). A leap frog scheme is used for the time stepping. Calculus costs are limited thanks to a time splitting technique that permits to compute the vertical shear of the current and its depth-averaged component separately with appropriate time steps.

The external forcings are of three types: river discharges, atmospheric fluxes and large scale inputs at open boundaries. The atmospheric forcings are provided by the 3-hours averaged outputs of the weather-forecast model Aladin. Open boundary conditions have a double purpose. They are first of all required to force the inner solution with external fields under incoming conditions. At the same time, they should allow waves to radiate out or water masses to leave the modelling domain under outgoing conditions, without any spurious reflections. Sea surface elevation and barotropic currents are given by the Flather radiative condition (Flather, 1976) using the numerical scheme recommended by Marsaleix *et al* (2006). Baroclinic velocities are given by a zero gradient condition in the direction normal to the boundary. Temperature and salinity boundary conditions use the same equations as for the inner solution but with an upstream advection scheme in order to advect external fields into the numerical area under inflow conditions. A boundary nudging layer enforces external forcing. In this layer, a restoring term $-\dfrac{\phi_F - \phi}{\tau_R(x,y)}$ is added to the right-hand-side of the model equations, where ϕ stands for tracers or velocities variables and subscript F refers to forcing terms. The restoring time scale $\tau_R(x,y)$ is such that this additional term progressively vanishes with the distance to the open boundaries. Practically, the nudging layer is roughly 15 grid nodes wide and $\tau_R(x,y)$ is of the order of one day on open boundaries.

The largest domain extends over the whole Northwestern Mediterranean sea (see Fig. 1) with a 3 km horizontal grid mesh and 41 vertical levels. The simulation over this domain lasts from January the 1st to April 10th 2005. It was obtained in the framework of the MFSTEP European project (http://www.bo.ingv.it/mfstep/), an operational oceanographic system delivering, every week, forecasts and hindcasts of the Mediterranean Sea. MFSTEP is based on a global Mediterranean Sea model assimilating sea level altimeter data, surface temperature and XBT temperature profiles. This project also involves several higher resolution embedded models downscaling the global solution to regional or coastal scales (Zodiatis *et al*, 2003; Auclair *et al*, 2006). Our model is actually directly derived from the MFSTEP regional model of the Northwestern Mediterranean Sea. This regional model has been specially replayed for the purpose of our study. We indeed performed a 4 months continuous run forced with meteorological and MFSTEP global re-analysis. This regional simulation provided high frequency (3 hours) outputs in order to force our coastal high resolution sub-models.

Instead of nesting the smallest domain of interest for our GAM study directly in this biggest domain, an intermediate domain, at the scale of the Gulf of Lion shelf (see Fig.1), is implemented with a 1 km horizontal grid mesh and 26 vertical levels. This domain permits to well represent the interactions between the general circulation (the Northern Current), the shelf circulation mainly induced by the winds and fresh waters mainly discharged from Rhone river.

Finally, the smallest modelling domain extends on the northern part of the inner shelf of the gulf of Lion, i.e. the GAM (see Fig. 1) with a 500 m horizontal grid mesh and 10 vertical levels. The simulation on this domain, lasting from March the 1st to April 10th 2005, permits a comparison between model results and in situ data during the 3 HYGAM cruises.

3. Results and discussions

In the following sections, we will discuss both *in situ* data and the corresponding model inputs or outputs. *In situ* data will be first compared to the model data. The degree of agreement will indicate to what extent model results can help in understanding observations.

3.1. Winds

The shelf circulation of the Gulf of Lions is dominated by wind. The later is locally highly variable and its rotational is known to induce specific mesoscale currents (Estournel *et al*, 2003) encroaching on GAM area. Three types of data are available: the coastal weather stations data, the meteorological station Batos (on board the ship) data, and the Aladin meteorological model data. On Fig. 3 and Fig. 4, the fit between each type of data can be pointed out; the Aladin model ones can then be used as realistic forcings of the *Symphonie* ocean circulation model.

After a period of relative atmospheric calm at the beginning of March, the period corresponding to the first HYGAM cruise (March 6-7) is characterized by strong winds which fluctuate between the north-north-west and north at La Grande Motte. These two directions correspond to very frequent winds in this region, called respectively Tramontane and Mistral. The Batos station data confirm the occurrence of these strong winds (between 5 and 15 m s^{-1}).

The Aladin model results are also in good agreement with the various types of data (for example, see Fig. 3 and Fig. 4 for the station of La Grande Motte).

In reality, orography plays a key role on wind fields : Tramontane blows between the Pyrenees and the Massif Central (Fig. 1), Mistral, in the Rhone valley, between the Massif Central and the Alps (Fig. 1). These two winds are then relatively well channelled, the Tramontane blowing most often from north-north-west on the west side of Gulf of Lion, and the Mistral, from the north on the east side of the Gulf of Lion. This typical situation occurs during the first HYGAM cruise. The GAM is at the convergence of these two winds. Fig. 5 shows how the east part of the gulf, on March 6, is under a Mistral of intensity above 10 m s^{-1}, how the west part is under a Tramontane of same intensity, and how the winds are nearly absent in the central part of the gulf.

After the first cruise, the winds intensity weakens until March 20 (Fig. 3), beginning of the second HYGAM cruise for which the sea state was nearly calm (slack sea at the beginning of the cruise). During this second cruise, the very good agreement between each type of data can be noticed (Fig. 3 and Fig. 4). It shows a drift from south to east winds and a progressive increase of the wind intensity up to 10 m s^{-1} at the end of the cruise (March 21).

The end of March is characterized by an important variability of the weather conditions, with alternations of calm periods (March 25), of east winds (March 26), of Tramontane (March 28), and of Mistral (March 31), with relatively strong intensities. At the beginning of April, the winds are from east and south-east, with strong intensities as high as 14 m s^{-1} measured and modelled on April the 2nd. These offshore winds can generate important swells from east to southeast with significant heights on the order of 2 to 3 m. In the following discussion, we will see that these swells take certainly an important part in the nearshore oceanic circulation. On April 5, at the beginning of the third HYGAM cruise, these south-eastern and eastern winds weaken and then strengthen at the end of the cruise, on April 6.

During the three HYGAM cruises, weather conditions were typical of this region (1. north and north-west winds, 2. fine weather, 3. offshore winds). The measured data should then permit to understand the oceanic circulation during such conditions.

3.2. Hydrology

Two types of hydrological data are available: the surface data acquired continuously by the thermosalinograph and the CTD data. Some representative data will be presented in the next paragraphs.

The salinity is relatively constant during the whole period and uniform for the studied region, except for some zones desalinated by the plumes of small coastal rivers. On the contrary, the temperature fluctuates strongly during the whole studied period, depending on the location. The CTD samplings (76 done during the three HYGAM cruises) clearly show this variability. On Fig. 6, temperature profiles measured during the three cruises at two stations, 7 in high seas (43°N15’-4°E02’), and 8 near the coast (43°N30’-4°E02’) (see positions on Fig. 2) are represented.

Because of a particularly cold winter during 2004-2005, the coastal waters are extremely cold at the beginning of March (9.7 °C at station 8 on March 6). The water column is vertically homogeneous, but we can note that the offshore waters are warmer (10.7 °C at station 7 on March 6). The model is consistent with these data (error < 0.2°C on Fig. 6 for H1), and allows then to better understand the situation. Fig. 7a displays the surface temperature modelled on March 6. Coastal waters are extremely cold (9.0°C). These waters are part of the Western Mediterranean Intermediate Water's (WIW's) formation (Dufau-Julliand *et al*, 2004). Warmer waters are brought due to a south flux creating an important thermic gradient (>2°C) between offshore and coastal waters (Fig. 7a). The data of the thermosalinograph (Fig. 7b) confirm this strong gradient.

On March 20, coastal waters have warmed up (11.3 °C at 10 m at station 8). The thermic gradient between offshore and coastal waters is now less pronounced (12.6 °C at 10 m at station 7). The fine weather period enhances this warming, and the water column stratification has begun (10.0 °C at 90 m at station 7). The model follows this warming up tendency. It displays the appropriate range of values, but does not reproduce the vertical gradient. The surface values (see Fig. 7c and Fig. 7d) are for example under-estimated, the difference being at least of 1.0 °C. In reality, the warmed layer is slightly too thick in the model. This might be caused by an inappropriate parameterisation of the attenuation of surface irradiance with depth in our model. This parameterisation is based on an exponential decay law, $e^{z/d}$, depending on a vertical scale parameter, $d=22m$, which roughly corresponds to the clear water case (case one) of the Jerlov water type classification (Apel, 1987). Actually one can expect nearshore waters to be turbid because of biogeochemical activities or suspended matter brought by rivers or bottom turbulence, and consequently, the vertical scale parameter used in our parameterisation to be much smaller. An adjusted value of this parameter might lead to a better representation of the warmed layer thickness. Nevertheless, the data from the thermosalinograph (Fig. 7d) confirm that warmer waters are again brought by an offshore flux.

On April 5, the warming goes on, and, for the first time, the coastal waters have the same temperature than the offshore waters (13.5-14.1 °C at the surface on Fig. 6). The model still slightly under-estimates this warming, especially near the coasts, but shows a horizontal homogenisation trend (Fig. 7e). The data from the thermosalinograph (Fig. 7f) again confirm the warming of the coastal waters and display relatively cold offshore waters, near 13.0 °C (principally south-west of the studied region). The CT7 H3 profile (Fig. 6) shows that the water column is relatively less stratified than 16 days before (0.9°C instead of 2.6°C between surface and bottom), the weather conditions having favoured vertical mixings. The model, which tends to be more vertically homogeneous, is then closer to reality.

3.3. Circulation

3.3.1. HYGAM 1

The ADCP data measured at 16 m depth along the first track of the HYGAM 1 cruise (between 8h00 on March 6 and 6h00 on March 7) are represented on Fig. 8. Results for data available every 4 m depth (figures not included) exhibit an important vertical homogeneity of the circulation. This vertical homogeneity is confirmed by representing vertically the data measured along transect 7-8 (south-north, longitude 4°02'E) on Fig. 9a and Fig. 9c. One can however note that the ADCP data are valid when located between 12 m above the bottom and 16 m under the sea surface. This implies that the ADCP gives generally valid data offshore of the 30 m bathymetry line. We then understand the utility of completing this data with model results.

The corresponding model results (shown on Fig. 10 at 12h00 on March 6 at 16 m depth) are very close to the in situ data. These model results are represented on Fig. 9b and Fig. 9d along the same transect than the data one and at 12 h on March 6. These figures confirm that the velocity fields are nearly homogeneous on the whole water column, and not only at the measured depths. The data measured at 16 m depth (Fig. 8) are then representative of the surface currents. This vertical homogeneity corresponds effectively to the temperature vertical homogeneity (see §3.2.), characteristic of the winter period. In a general case, and particularly in summer, we will have to be very cautious when interpreting the currents measured at 16 m depth as representative of the surface currents.

Near the bottom, under 40 to 50 m depth, the model shows however that the currents tend to decrease, and even reverse. One can for example remark the reverse under 60 m depth (Fig. 9c and Fig. 9d) on the southern part of the transect 7-8 (latitude 43.25°N). This particular case is however well detected in the measurements (Fig. 9 a).

The near-perfect consistency between observed and simulated data allows then a detailed analysis. On Fig. 8, the data of the three western transects show currents toward the west and the southwest-west after the 40 m-isobath. The model reproduces well this flux due to the Ekman drift created by the northwest wind (Tramontane, see Fig. 5) present on the western part of the GAM. Data prove that these currents can locally reach 0.20 m s^{-1} whereas the model, which has a tendency to smooth extreme values, simulates a current near 0.12 m s^{-1}. Closer to the coast (before the 40 m-isobath), sparse data exhibit currents in the opposite direction with very weak intensity. The model gives also very low values of velocities nearshore (before the 40 m-isobath), where we get closer to the atmospheric calm zone (see Fig. 5).

As the Tramontane controls the circulation in the west part of the GAM, the Mistral (north wind on Fig. 5) controls the circulation of the east part of the GAM. The data of the three eastern transects show currents toward the east and the southeast-east between the 20 m- and 60 m-isobaths. The data show these currents can locally reach 0.30 m s^{-1}. The model reproduces well this waters export of GAM toward the east with a mean flow on the order of 0.20 m s^{-1} focused between the 20 m- and 60 m-isobaths.

In the central part of the GAM, the circulation understanding becomes less direct. Indeed, whereas the atmospheric flux is mainly southward, the oceanic flux seems northward. More precisely, the more-offshore transect data show currents globally westward, and even locally northward (longitude 4°05' E, with an intensity up to 0.30 m s^{-1}). The eastern transect exhibits a break at 60 m-isobath between the nearshore waters going eastward and the offshore ones going westward. The transect 7-8 (Fig. 9) also displays a change in direction. The southern data of this transect (up to 43.30°N) show a northward current at 0.16 m s^{-1}. Fig. 9a and Fig. 9c show between 43.30°N and 43.35°N a north-westward current that can reach 0.28 m s^{-1}. Weaker currents are measured between 43.35°N and 43.40°N. Nearshore, north of the latitude 43.40°N, the current is reversed, going eastward at 0.20 m s^{-1}. The model gives results close to the observations with a north-westward current south of the latitude 43.40°N, and an eastward current north of this latitude (Fig. 9 b and Fig. 9d).

With this typical meteorological situation of Tramontane (north-northwest wind) and Mistral (north wind), respectively channelled west and east of the GAM, an important oceanic circulation occurs northward and north-westward in the centre part of the GAM. This circulation splits, turning toward west and southwest-west in the western part of the GAM and turning eastward in the eastern part of the GAM.

During the Sarhygol 3 cruise (June 13-15 2000), concerning the whole Gulf of Lion's shelf, with the same meteorological conditions (channelled Tramontane and Mistral), Petrenko *et al* (2005) observed the same northward flux between longitudes 3.9°E and 4.3°E at latitude 43.1°N. They interpreted this flux to be an intrusion of the Northern Current, MAW (Modified Atlantic Water) general circulation current located on the continental slope (near latitude 42.7°N, longitude 4.0°E). Estournel *et al* (2003) explained by modelling that such intrusions in the middle of the shelf are due to the water pumping created by a cyclonic circulation on the western side of the gulf of Lion and an anticyclonic circulation on the eastern side. Estournel *et al* (2003) found that these rotating circulations are wind-driven, the former by the Tramontane, and the latter by the Mistral. The two rotating circulations join in the middle of the gulf of Lion, it means in the GAM.

HYGAM 1 observations and the corresponding modelling confirm these previous studies. We also show the consequences at the GAM scale. The origins of the south flux are better understood, and the consequence is an important thermic gradient (>2°C) between offshore and coastal waters (see §3.2. and Fig. 7 and Fig. 8). These warmer waters come actually from the Northern Current, warmer in winter than the surrounding waters, and particularly, than the nearshore waters.

After the HYGAM 1 cruise, the model shows a persistence of the south flux laterally evacuated. The lateral drift toward southeast to east in the eastern part of the GAM is the only one to persist after March 9. Then, until March 20, the currents intensity is weak, corresponding to the weak winds intensity (see §3.1.). This period between the first two cruises favours also the first spring warmings (see §3.2.).

3.3.2. HYGAM 2

For this second cruise, the model results are less coherent with the data.

Nearshore until 70 m-isobath, currents are globally longshore (they follow the isobaths) westward (Fig. 11). The model reproduces quite well this longshore flux (Fig. 12). This might be explained by the sum of two effects. The first is due to the south winds with weak intensity (≤ 4 m s^{-1}). These winds pile water on the shoreline and induce a raise of the sea surface elevation, estimated by the model to be 3 to 4 cm between the 70 m- isobath and the shoreline. Such a surface elevation slope is sufficient to create a geostrophic current on the order of 0.15 to 0.20 m s^{-1}. The model proves that these longshore currents, in quasi geostrophic equilibrium with the surface pressure gradient, can be accelerated by southeast winds which strengthen during the cruise. These simulated currents can reach 0.30 m s^{-1} (see Fig. 12, latitude 43.3°N, longitude 4.1°E).

Offshore, after 70 m-isobath, the model is less coherent with the measurements. In order to complete the observation of the south flux measured on March 21, 0 h, on the southern southwest transect (see Fig. 11), we decided to modify our plan by continuing southward, until latitude 43°10'N, the north-south transect 8-7 (longitude 4°02'E). The southward transect ended 6 h after the first path at the station 7 and does not confirm this south flux. By analysing Fig. 13, we can however note the consistency between the model results and the measurements along this longer transect 8-7. South of the station 7 (latitude < 43.25°N), the observed currents (westward) are quite different from the model ones (eastward), but the current intensities are in fact quite low (< 0.05 m s^{-1}). North of the station 7, between the latitudes 43.27°N and 43.34°N, a north-eastward current (~ 0.35 m s^{-1}) is observed, whereas the model shows the same current slightly more south (between the latitudes 43.24°N and 43.30°N). On Fig. 12, it is clear that this current takes part to the recirculation of nearshore waters, westward advected north of latitude 43.34°N. This longshore advection is particularly important (~ 0.30 m s^{-1}) westward between latitudes 43.34°N (70 m-isobath) and 43.40°N (40 m-isobath).

Contrary to HYGAM 1 cruise, the meteorological situation is less pronounced and fluctuates, leading to a more difficult analysis of the measured currents. Moreover, the model is less constrained by this type of inputs, and thus the model results can be less realistic. One can remark that the model failed in reproducing the south-eastward current measured at the southeast of our observed domain.

Whereas the meteorological conditions are very different from the first cruise ones, one can note the south flux which similarly advects the warmer waters in the GAM (see §3.2).

At the end of the cruise and until March 28, the model exhibits the development of a strong westward nearshore drift (between 0 and 30 m isobaths). This drift can reach 0.60 m s^{-1} and is also modelled during the HYGAM 2 cruise with an intensity of 0.30 m s^{-1} (see Fig. 13c at latitude 43.5°N). It is maintained by south to east atmospheric fluxes. This state changes completely in few hours on March 28. North winds at the end of March create a circulation similar to the one described for HYGAM 1 cruise. At the beginning of April, the south-southeastern winds again generate this strong westward nearshore drift. Before the HYGAM 3 cruise, the winds weaken, as well as the currents.

3.3.3. HYGAM 3

On April 5, the meteorological conditions are calm and the measured currents, weak (< 0.20 m s^{-1} on Fig. 14). The simulated currents at 16 m (Fig. 15) are coherent with the measured ones. As for HYGAM 2 cruise, the south-southeastern strong winds, preceding the cruise, piled the waters inside the gulf, creating a raise of the sea surface elevation on the order of 5 cm between the shoreline and the 90 m-isobath (see Fig. 15). The westward currents parallel to the isobaths, measured and simulated, can then be issued, as a first approximation, from the geostrophic equilibrium imposed by this slope. The analysis of the currents at 16 m-depth (Fig. 14 and Fig. 15) does not allow to go further than the correlation between data and model results.

A vertical section (Fig. 16) gives more information. Because of a sediment sampling plan and of the numerous fishing nets on the zone, this section was obtained on the north-south profile, longitude 4°07'E, instead of 4°02'E, as for HYGAM 1 and 2 (Fig. 9 and Fig. 13). The data exhibit currents at 0.10 to 0.15 m s^{-1} toward north-west-west, quite homogeneous between the 16 m-depth and the deeper ADCP cell (at least 12 m above the seafloor). The model tends to concentrate this motion quantity toward north-west-west between the 10 to 25 first meters depth. Under this surface moving layer, water is quite static, and even oriented in the opposite direction near the bottom.

In fact, these discrepancies might be caused by an important swell before and during the cruise. To go further than the first seasick impression onboard, we decided to study the waves data. The measured waves data are either inexistent (the Sète Datawell station was down) or very offshore (Météo-France station at latitude 42.0°N). This latter permits however Météo-France to run the VAGMED model. We acquired their results for March-April 2005 period. Fig. 17 shows results close to the Station 7 at 43.25°N, 4.00°E. For March, except for short events of south to east waves, the GAM is nearly not under the influence of waves. For the first two HYGAM cruises, the waves are very weak. On the contrary, at the beginning of April, the south-southeastern winds generate higher (> 1 m) and longer (~8 s) waves. These swells continue during the whole HYGAM 3 cruise, and even strengthen at the end.

A fundamental issue is to know what are the consequences of such swells on the oceanic circulation. The results of the third cruise show the limitations of the followed methodology and raised some questions which will be discussed in section 4.

In one way, the measured data need to be completed by data near the surface and the bottom, and closer to the coast. Indeed, the swell will certainly have the greatest influence on these zones. In the other way, the numerical model used here does not take into account the swell effects on the circulation. We will see in the next section what is planned to improve these two aspects.

4. Conclusions and Perspectives

This observation and modelling work at an intermediate scale between nearshore (e.g. Meulé *et al*, 2001) and coastal (e.g. Petrenko *et al*, 2005) studies is one of the first experiments for this region. It permits to obtain a quite realistic description of the oceanic circulation during the 39 days of simulation, including the 6 days of observations. We can note:

- the important variability of the oceanic circulation at this scale,
- the importance of the winds and of their horizontal gradients, inducing coherent structures, both at GAM and continental shelf scales,
- the interactions with the general oceanic circulation (intrusions of the Northern Current),

- longshore currents achieving the geostrophic equilibrium with the surface slope, itself created by offshore winds,
- important heat exchanges, offshore toward the coast by offshore south fluxes,
- the formation of cold waters near the shoreline, certainly supplying the WIW,
- the relative discrepancies between the model and the data when swell is present.

In order to better understand the GAM hydrodynamics, many improvements are to be achieved, in modelling as well as in observation.

4.1. Modelling improvements

This paper shows that models of costal oceanic circulation, as *Symphonie*, are able to well reproduce the circulations inferred by winds at different scales, included shelf circulations interacting with general circulation. Nesting modelling is an undeniable progress realised during the last years. The differences of thermohalines and sea surface elevation also permit to generate important circulations at this scale.

Beyond the progress already obtained and awaited in numerical aspects (numerical schemes, nesting methods …) and beyond the realism of forcings (atmospheric and large scale circulations), important progresses are still to achieve in order to take into account the physical phenomena.

For example, taking into account the astronomical and atmospheric tides is quite important. Whereas these tides generate only weak velocities (a few cm s^{-1}), the setups are rather important (on the order of 50 cm, Lyard, pers com), when the coefficients tides are high, and especially when atmospheric depression occurs. These setups have a real impact on the littoral in terms of flooding (storm surges). For future studies we plan to take into account high frequency barotropic processes, induced by tides and/or atmospheric pressure, in order to focus on storms and their potential consequences on littoral.

In the same idea, we are convinced that it is important to take into account the swell in a zone like the GAM. Among the major known wave effects on the ocean circulation, one can note:

- the increase of the surface roughness in the presence of surface waves (Donelan *et al*, 1993),

- the modification of the bottom stress by the wave-current interactions in shallow waters (e.g. Christofferson and Jonsson, 1985),

- the interactions between wave- and wind/buoyancy- driven currents via the radiation stresses (Longuet-Higgins and Stewart, 1962a) or the vortex force (Garrett, 1976 ; Huang, 1979),

- the Coriolis effect on the surface wave-induced currents (Jenkins, 1987) and the Stokes drift caused by the balance between Coriolis forces -which result from the mean and wave induce motions-, and the surface wind stress (modified Ekman equations) (Huang, 1971),

- the modification of the bottom and surface boundaries conditions for the turbulent kinetic energy (Terray et al, 1995; Mellor and Blumberg, 2004).

In order to study 3D hydrodynamics of inner shelf zones such as the GAM, a three dimensional model taking into account these wave effects at intermediate scale should be implemented. Following the physics described by Mellor (2003), the three dimensional effects of the waves are introduced in the coastal circulation model. With this approach, new forcing terms appear in the primitive equations. These forcing terms are mainly the gradient of the 3D radiation stresses, corresponding to those given by Longuet-Higgings and Stewart (1961a, 1962b) and Phillips (1966) in a 2D integrated model. Moreover, the surface and bottom stresses and the turbulent kinetic energy transport equation should be modified.

This perspective work is going to be achieved using the wave propagation model *REF/DIF* (Kirby and Dalrymple, 1983) to compute the wave characteristics used to force the coastal circulation model *Symphonie*. Preliminary tests on academic cases are already done (Denamiel *et al*, 2005). Fig. 17 shows that the swell events are quite rare on March-April 2005 period. However, during swell events as the one encountered for the HYGAM 3 cruise, the oceanic circulation at the GAM scale is undoubtedly to be modelled with the swell effects. In real, as for the tides, the swell effects are the most important during the south to southeast storms. The next step of this work should be the implementation of "*Symphonie modified by wave effects*" for such realistic extreme events.

4.2. Observation improvements

For the observations, the boat surveys, similar to the ones of the HYGAM cruises, are insufficient, even if they deliver precious information. They do not provide data for the few meters near the surface nor near the bottom. The lack of data between the shore and the 20 m-isobath complicates the comprehension of the continuity between the inner shelf and the littoral. The observations are also problematic because of the highly transitory character of the circulation at this scale. The HYGAM cruises experiment however shows that the structures are coherent and persistent enough to be measured by such surveys.

To complete these surveys, fixed observation stations are needed. On the continental shelf, it is difficult to maintain a bottom ADCP station because of intensive trawling. After negotiations with fishing comities and authorities, an ADCP (RDI 300 kHz with a wave module protected in a bottom mount) will be deployed in 2007 at 3°52'E, 43°15'N (station 5 on Fig. 2). This ADCP will allow to realize time series of vertical profiles of currents and swell characteristics every hour during a few months. A Seabird pressure sensor will also be installed on an artificial reef at 3°52'E, 43°26'N (station 6 on Fig. 2). It will measure time series of setup and non directional characteristics of swells, also every hour during a few months. For the littoral scale, a pressure sensors net, two Nortek ADVs and two ADCPs (RDI 600 kHz with wave modules), will be deployed on various beaches of the GAM. This effort made for the observations will permit to better describe the hydrodynamics of the GAM and to validate the numerical models, especially during the storms events.

4.3. Future applications

The improvement of observation and modelling tools at this scale is an important challenge for the next years. Applications are numerous. The Montpellier sewages are dumped since 2005 by a pipeline 10 km south of Palavas-Les-Flots, under 30 m of bathymetry (in the middle of the GAM). Their dispersion is a problem which needs a precise knowledge of the hydrodynamics. The small costal rivers, Mosson and Lez at Palavas-les-Flots, and Vidourle near La Grande-Motte (see locations on Fig. 2), also drain waters in urban and agricultural watersheds subject to contamination hazards. In case of important floods, the rivers plumes are subject to the GAM hydrodynamics. The knowledge of the GAM hydrodynamics is then useful for computing the contamination hazards.

This hydrodynamics also plays an important role for the computation of the submersion and erosion hazards. The submersion events are known to occur in the region during the south to southeast storms. During these events, the setups induced by the winds, by the tides and by the swells cumulate. The offshore atmospheric fluxes also lead to important precipitations. The GAM littoral is more often formed by beach ridges and low and lagoonar zones. These two factors aggravate the littoral submersion risks. For the submersion hazards computation, one understands the necessity to integrate tides and swells in the models and to measure the setups.

Except for the Espiguette cape, near Port-Camargue (see Fig. 2), the GAM littoral is also subject to an intense erosion. The sand sedimentary transport study is usually done at the littoral scale (e.g. Tessier *et al*, 2000 ; Meulé *et al*, 2001 ; Certain *et al*, 2005a, 2005b). These studies consider the littoral zone as a cell more or less isolated from offshore, with mainly longshore fluxes. It however seems important to evaluate cross-shore fluxes toward the offshore zone. Such fluxes certainly occur during south to east storms and might lead to sand lost beyond the coastal zone. This sand will then not contribute anymore to the coastal morphodynamics. To evaluate this flux, one will have to pursue studies such as the one presented in this paper, and more especially during storms.

In a region where tourism and littoral urbanisation impacts are fundamental, the society expects tools to evaluate the hazards (contamination, erosion, or submersion). The scientific knowledge is then expected and studies such as this one go in this way.

Acknowledgements

The cruises and study were financed by the French National program PATOM. We are grateful to the crews of the Téthys II. Lots of thank to Jean-Luc Fuda and the Centre d'Océanologie de Marseille for the lending of the CTD probe. We thank Gilles Rougier, Julie Gatti, Pierre-Michel Theveny, Eric Berthebaud and Florent Lyard who have participated to the HYGAM cruises.

References

Apel, JR., 1987. Principles of Ocean Physics. *International Geophysics Series, Vol. 38, Academic Press (New York). 634 pp.*

Auclair, F., Marsaleix, P., De Mey, P., 2003. Space-time structure and dynamics of the forecast error in a coastal circulation model of the Gulf of Lions. *Dynamics of Atmospheres and Oceans* 36, 309-346.

Auclair, F., Estournel, C., Marsaleix, P., Pairaud, I., 2006. On coastal ocean embedded modeling. *Geophysical Research Letters*, in press.

Blumberg, A. F. and Mellor, G. L., 1987. A description of a three-dimensional coastal ocean circulation model, in Three-Dimensional Coastal ocean Models, edited by N. Heaps, 208 pp., American Geophysical Union.

Certain, R., Meulé, S., Rey, V., Pinazo, C., 2005a. Wave transformation on a microtidal barred beach (Sète, France). *Journal of Marine Systems* 58(1-2), 19-34.

Certain, R., Tessier, B., Barusseau, J.-P., Courp T. and Pauc H., 2005b. Sedimentary balance and sand stock availability along a littoral system. The case of the western Gulf of Lions littoral prism (France) investigated by very high resolution seismic. *Marine and Petroleum Geology* 22(6-7), 889-900.

Christoffersen, J. B. and Jonsson, I. G., 1985. Bed friction and dissipation in a combined current and wave motion. *Ocean Engineering* 12(5), 387-423.

Conan, P. and Millot, C., 1995. Variability of the northern current off Marseilles, western Mediterranean Sea, from February to June 1992. *Oceanologica Acta* 18(2), 193-205.

Delleville, S., 1997. Contribution à la modélisation de la dynamique marine d'été du golfe du Lion. Application d'un modèle emboité passif. Thèse, Université d'Aix-Marseille II.

Denamiel, C., Bouchette, F., Leredde, Y., Marsaleix, P., 2005. Three-dimensionnal coupled modeling of wave- and wind/buoyancy- driven currents: An application in the Gulf of Aigues-Mortes (NW Mediterranean sea, France). European Geosciences Union, General Assembly. Vienna, Austria, 24 - 29 April 2005. Geophysical Research Abstracts, 7, 03268.

Donelan, M. A., Dobson, F. W., Smith, S. D. and Anderson, R. J., 1993. On the dependence of sea surface roughness on wave development. *Journal of Physical Oceanography* 23, 2143-2149.

Dufau-Julliand, C., Marsaleix, P., Petrenko, A. and Dekeyser, I., 2004. Three-dimensional modeling of the Gulf of Lion's hydrodynamics (northwest Mediterranean) during Jannuary 1999 (MOOGLI3 Experiment) and late winter 1999: Western Mediterranean Intermediate Water's (WIW's) formation and its cascading over the shelf break. *Journal of Geophysical Research* 109, C11002.

Durrieu de Madron, X., Radakovitch, O., Heussner, S., Loye-Pilot, M. D. & Monaco, A., 1999. Role of the climatological and current variability on shelf-slope exchanges of particulate matter: Evidence from the Rhône continental margin (NW Mediterranean). *Deep-Sea Research* 46, 1513-1538.

Echevin, V., Crépon, M. and Mortier, L., 2003. Interaction of a coastal current with a gulf : application to the shelf circulation of the Gulf of Lions in the Mediterranean Sea. *Journal of Physical Oceanography* 33, 188-206.

Estournel, C., Kondrachoff, V., Marsaleix, P., Vehil, R., 1997. The plume of the Rhone: numerical simulation and remote sensing. *Continental Shelf Research* 17(8), 899-924.

Estournel, C., Durrieu de Madron, X., Marsaleix, P., Auclair, F., Julliand, C., Vehil, R., 2003. Observation and modelisation of the winter coastal oceanic circulation in the Gulf of Lions under wind conditions influenced by the continental orography (FETCH experiment). *Journal of Geophysical Research* 108(C3), 8059.

Estournel, C., Zervakis, V., Marsaleix, P., Papadopoulos, A., Auclair, F., Perivoliotis, L., Tragou, E., 2005. Dense water formation and cascading in the Gulf of Thermaikos (North Aegean) from observations and modelling, *Continental Shelf Research* 25, 2366-2386

Flather, R. A., 1976: A tidal model of the northwest european continental shelf. Mem. Soc. R. Sci. Liege, Ser 6, 10, 141-164.

Garrett, C., 1976. Generation of Langmuir circulations by surface waves - a feedback mechanis. *Journal of Marine Research* 34 :117-130.

Gaspar, P., Gregoris, Y. & Lefevre, J. M., 1990. A simple eddy kinetic energy model for simulations of the oceanic vertical mixing tests at station Papa and long-term upper ocean study site. *Journal of Geophysical Research* 95, 179-193.

Huang, N.E., 1971. Derivation of the stokes drift for deep water random gravity wave field. *Deep-Sea Research* 18, 255-259.

Huang, N.E., 1979. On surface drift currents in the ocean. *Journal of Fluid Mechanics* 91, 191-208.

Jenkins, A.D., 1987. Wind and wave induced currents in arotating sea with depth-varying eddy viscosity. *Journal of Physical Oceanography* 17(7), 938-951.

Kirby, J.T. and Dalrymple, R.A., 1983. A parabolic equation for the combined refraction diffraction of Stokes waves by midly varying topography, *Journal of Fluid Mechanics* 136, 543-466.

Lapouyade, A. & Durrieu de Madron, X., 2001. Seasonal variability of the advective transport of particulate matter and associated organic carbon in the Gulf of Lions (NW Mediterranean). *Oceanologica Acta* 24, 295-312.

Longuet-Higgins, M.S. and Stewart, R.W., 1961. The changes in amplitude of short gravity waves on steady non uniform currents. *Journal of Fluid Mechanics* 10, 529-549.

Longuet-Higgins, M.S. and Stewart, R.W., 1962a. Radiation stress and mass transport in gravity waves, with application to 'surf beats'. *Journal of Fluid Mechanics* 13, 481-504.

Longuet-Higgins, M.S. and Stewart, R.W., 1962b. Radiation stresses; a physical discussion, with applications. *Deep-Sea Research* 11, 529-562.

Marsaleix, P., Auclair F., Estournel C., 2006. Considerations on open boundary conditions for regional and coastal ocean models. *Journal of Atmospheric and Oceanic Technology*. In press.

Mellor, G., 2003. The three dimensional current and surface wave equations. *Journal of Physical Oceanography* 33, 1978-1989.

Mellor, G. and Blumberg, A.F., 2004. Wave breaking and ocean surface layer thermal response. *Journal of Physical Oceanography* 34, 693-698.

Meulé, S., C. Pinazo, C. Degiovanni, J.-P. Barusseau and L. Maurice, 2001. Numerical study of sedimentary impact of a storm on a sand beach simulated by hydrodynamic and sedimentary models. *Oceanologica Acta* 24(5), 417-424.

Millot, C., 1990. The Gulf of Lion's hydrodynamics. *Continental Shelf Research* 10(9-11), 885-894.

Monaco, A., Courp, T., Heussner, S., Carbonne, J., Fowler, S.W., Deniaux, B., 1990. Seasonality and composition of particulate fluxes during ECOMARGE-I, western Gulf of Lions. *Continental Shelf Research* 10 (9–11), 959–987.

Naudin, J. J., Cauwet, G., Fajon, C., Oriol, L., Terzic, S., Devenon, J. L. & Broche, P., 2001. Effect of mixing on microbial communities in the Rhone River Plume. *Journal of Marine System* 28, 203-227.

Pairaud, I., Auclair, F., 2005. Combined wavelet and principal component analysis (WEof) of a scale oriented model of coastal ocean gravity waves. *Dynamics of Atmospheres and Ocean* 40, 254-282.

Petrenko, A., Leredde, Y. and Marsaleix, P., 2005. Circulation in a stratified and wind-forced Gulf of Lions, NW Mediterranean Sea: in-situ and modeling data. *Continental Shelf Research* 25, 7-27.

Phillips, O.M., 1966. The dynamic of the upper ocean, Cambridge University Press, London, 336 pp.

Raimbault, P., Durrieu de Madron X, 2003. Research activities in the Gulf of Lion (NW Mediterranean) within the 1997-2001 PNEC project. *Oceanologica Acta* 26, 291-298.

Shchepetkin, A.F., McWilliams, J.C., 2005: The regional oceanic modeling system (ROMS): A split-explicit, free-surface, topography-following-coordinate oceanic model.

Ocean Modelling 9,347-404.

Terray, E.A., Donelan, M.A., Agrawal, Y.C.,Drennan, W.M., Kahma, K.K.,Williams, III A.J.,Hwang, P.A., Kitaigorodskii, S.A., 1995. Estimates of kinetic energy dissipation under breaking waves. *Journal of Physical Oceanography* 26, 792-590.

Tessier, B., Certain, R., Barusseau, J-P. et Henriet, J.P., 2000 . Évolution historique du prisme littoral de l'étang de Thau (Sète, Sud-Est de la France). Mise en évidence par sismique réflexion THR, *C. R. Acad. Sci. Paris, Sciences de la Terre et des planètes/ Earth and Planetary Sciences* 331, 709-716.

Ulses, C., Grenz, C., Marsaleix, P., Schaaff, E., Estournel, C., Meulé, S., Pinazo, C., 2005. Circulation in a semi-enclosed bay under influence of strong freshwater input. *Journal of Marine Systems* 56(1-2), 113-132.

Zodiatis, G., Lardner, R., Georgiou, G., Demirov, E., Pinardi, N., Manzella, G., 2003. The Cyprus coastal ocean forecasting and observing system, a key component in the growing network of European ocean observing systems. *Sea Technology* 44(10), 10-15.

Figure captions

Fig. 1: Geographical situation of this study. Frames of the three nested modeling grids. Bathymetry of the largest modeling grid (isolines every 500 m).

Fig. 2: Geographical situation of this study with the cities. Bathymetry (isolines, 20 m to 80 m). HYGAM cruises main stations (squares 1 to 8) and tracks (straight lines).

Fig. 3: Wind speed measured at La Grande Motte (solid line), modeled by Aladin at the same location (dotted line) and measured on the RV during the cruises (+).

Fig. 4: Wind direction measured at La Grande Motte (solid line), modeled by Aladin at the same location (dotted line) and measured on the RV during the cruises (+).

Fig. 5: Wind (arrows and colors ; m s^{-1}) modeled by Aladin at 12h00 on March 6.

Fig. 6: Temperature profiles :

- measured at station 8 during HYGAM 1, at 18h10 on March 6 (CTD8 H1), during HYGAM 2, at 6h33 on March 20 (CTD8 H2), during HYGAM3, at 20h11 on April 5 (CTD8 H3),
- simulated at the same place and times (MOD8 H1, MOD8 H2, MOD8 H3) ,
- measured at station 7 during HYGAM 1, at 11h04 on March 6 (CTD7 H1), during HYGAM 2, at 0h16 on March 21 (CTD7 H2), during HYGAM3, at 8h50 on April 5 (CTD7 H3),
- simulated at the same place and times (MOD7 H1, MOD7 H2, MOD7 H3) .

Fig. 7: Surface temperature (°C) :

(a) modeled by *Symphonie* at 12h00 on March 6,
(b) measured by the Téthys' thermosalinograph on March 6 (same color scale than (a)),
(c) modeled by *Symphonie* at 12h00 on March 20,
(d) measured by the Téthys' thermosalinograph on March 20 (same color scale than (c)),
(e) modeled by *Symphonie* at 21h00 on April 5,
(f) measured by the Téthys' thermosalinograph on April 5 (same color scale than (e)).

Fig. 8: Currents measured at 16 m depth along the cruise track between 8h00 on March 6 and 6h00 on March 7.

Fig. 9: Vertical sections (depth vs. latitude) of the currents (colors, m s^{-1}) on March 6 along transect 8-7 (longitude 4°02'E): (a) observed eastward component, (b) simulated eastward component, (c) observed northward component, (d) simulated northward component

Fig. 10: Currents (colors, m s^{-1}) modeled by *Symphonie* at 12h00 on March 6 at 16 m depth.

Fig. 11: Currents measured at 12 m depth along the cruise track between 17h00 on March 20 and 15h00 on March 21.

Fig. 12: Currents (colors, m s^{-1}) modeled by *Symphonie* at 06h00 on March 21 at 16 m depth.

Fig. 13 : Vertical sections (depth vs. latitude) of the currents (colors, m s^{-1}) on March 21 along transect 8-7 (longitude 4°02'E): (a) observed eastward component, (b) simulated eastward component, (c) observed northward component, (d) simulated northward component.

Fig. 14: Currents measured at 16 m depth along the cruise track beetween 6h00 on April 5 and 5h00 on April 6.

Fig. 15: Currents (colors and arrows, m s^{-1}) and surface elevation (black isolines, cm) modeled by *Symphonie* at 12h00 on April 5 at 16 m depth.

Fig. 16 : Vertical sections (depth vs. latitude) of the currents (colors, m s^{-1}) on April 5 along transect 8-7 (longitude 4°02'E): (a) observed eastward component, (b) simulated eastward component, (c) observed northward component, (d) simulated northward component

Fig. 17 : Total wave characteristics simulated by Vagmed Météo-France model at 43.25°N, 4.00°E

Figures

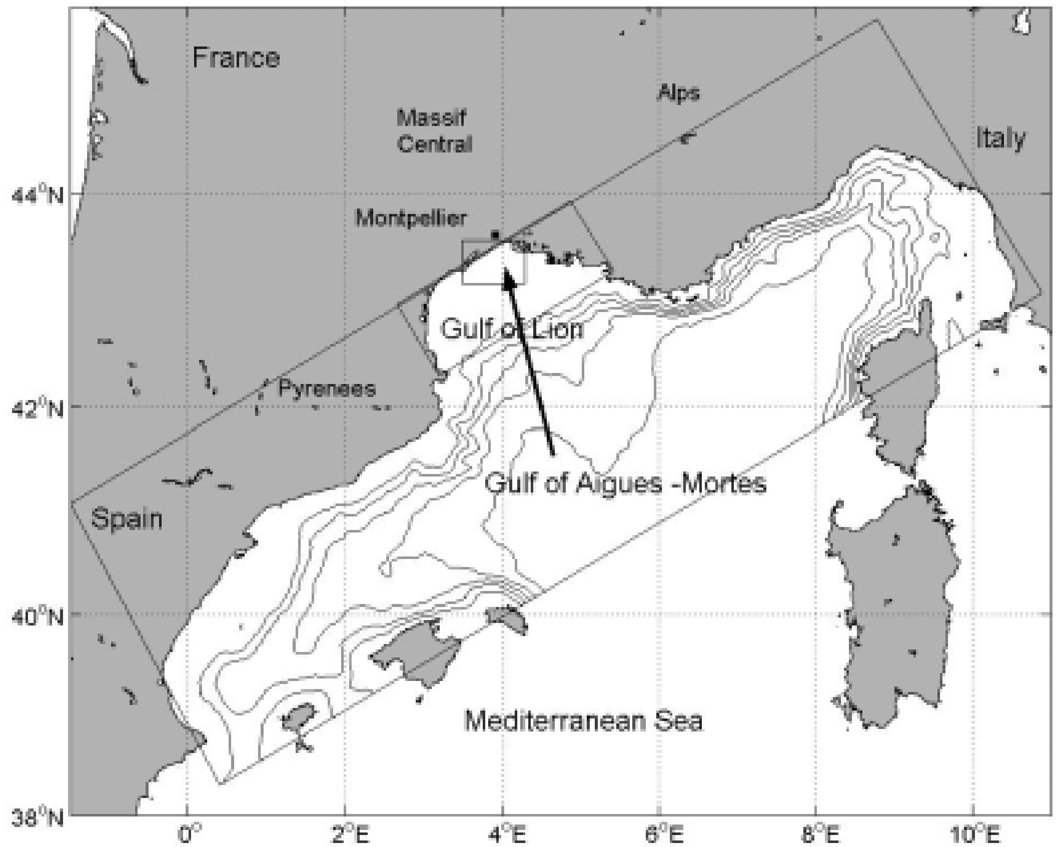

Fig. 1: Geographical situation of this study. Frames of the three nested modeling grids. Bathymetry of the largest modeling grid (isolines every 500 m).

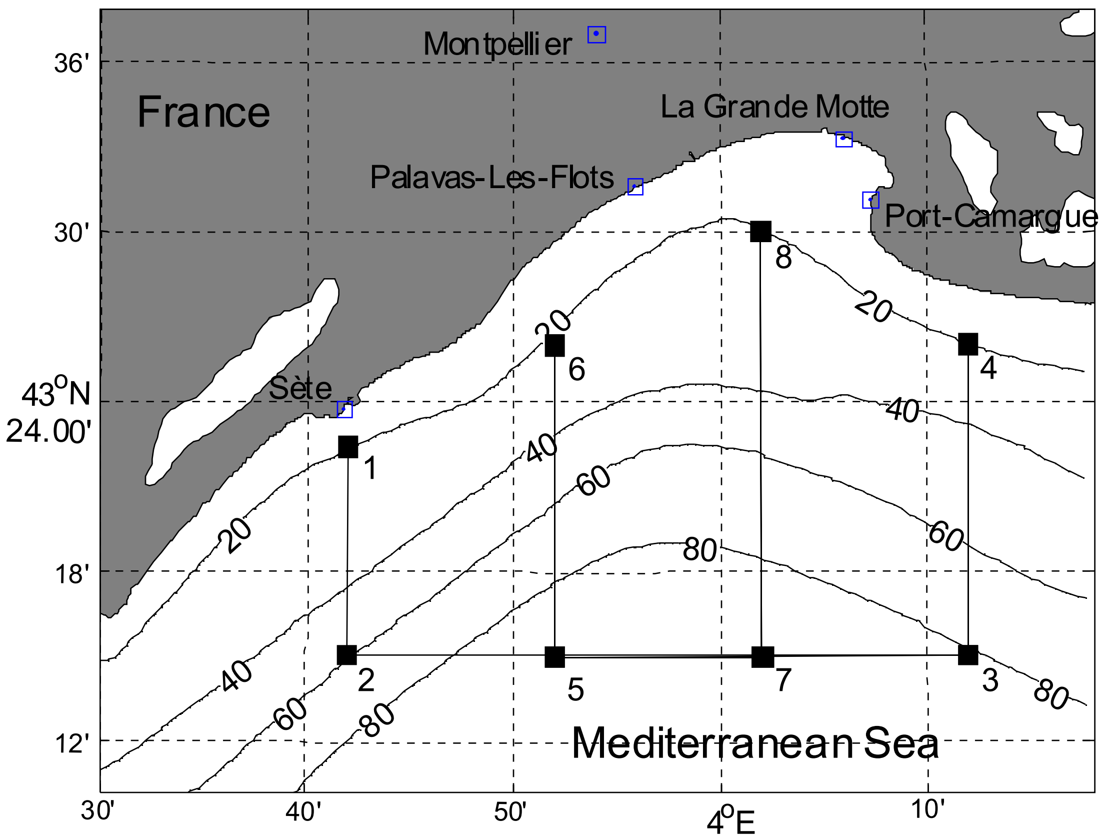

Fig. 2: Geographical situation of this study with the cities. Bathymetry (isolines, 20 m to 80 m). HYGAM cruises main stations (squares 1 to 8) and tracks (straight lines).

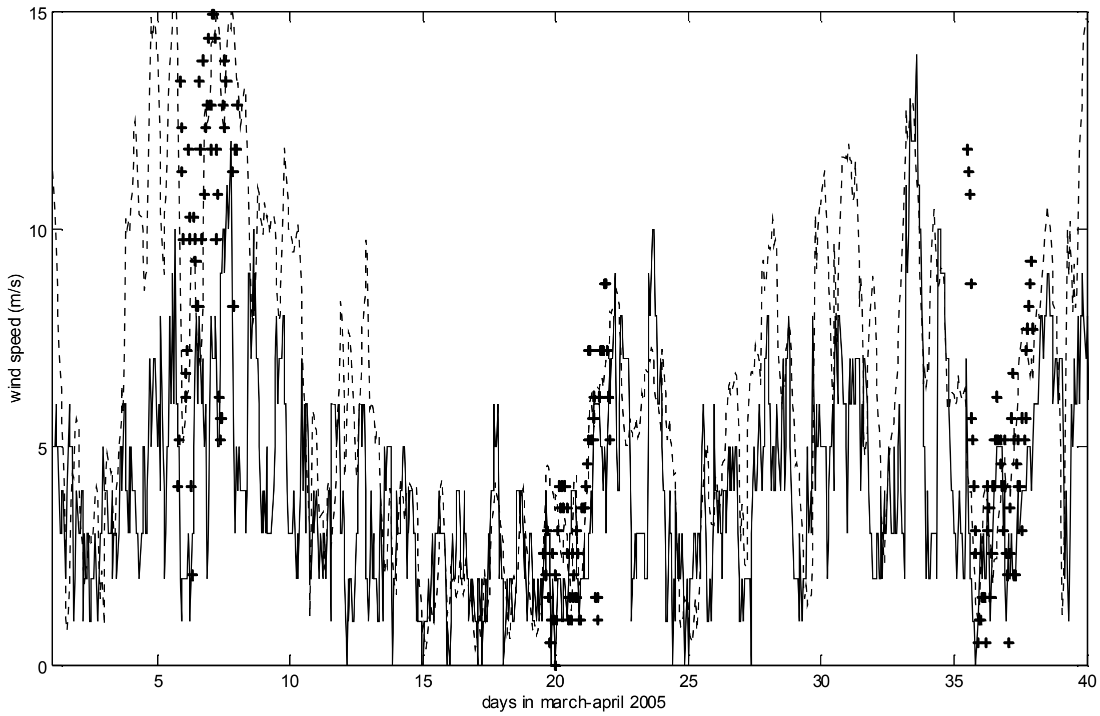

Fig. 3: Wind speed measured at La Grande Motte (solid line), modeled by Aladin at the same location (dotted line) and measured on the RV during the cruises (+).

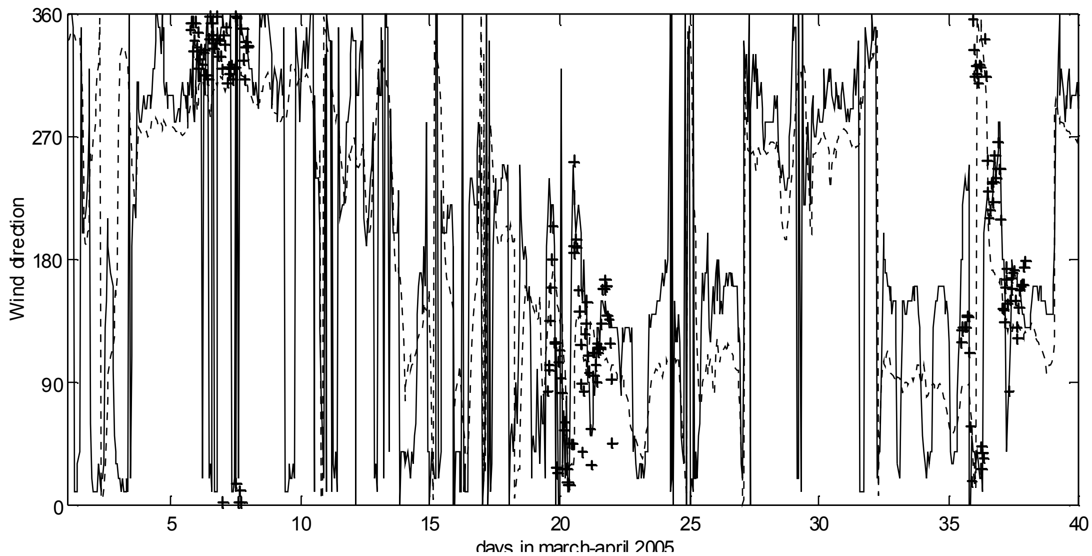

Fig. 4: Wind direction measured at La Grande Motte (solid line), modeled by Aladin at the same location (dotted line) and measured on the RV during the cruises (+).

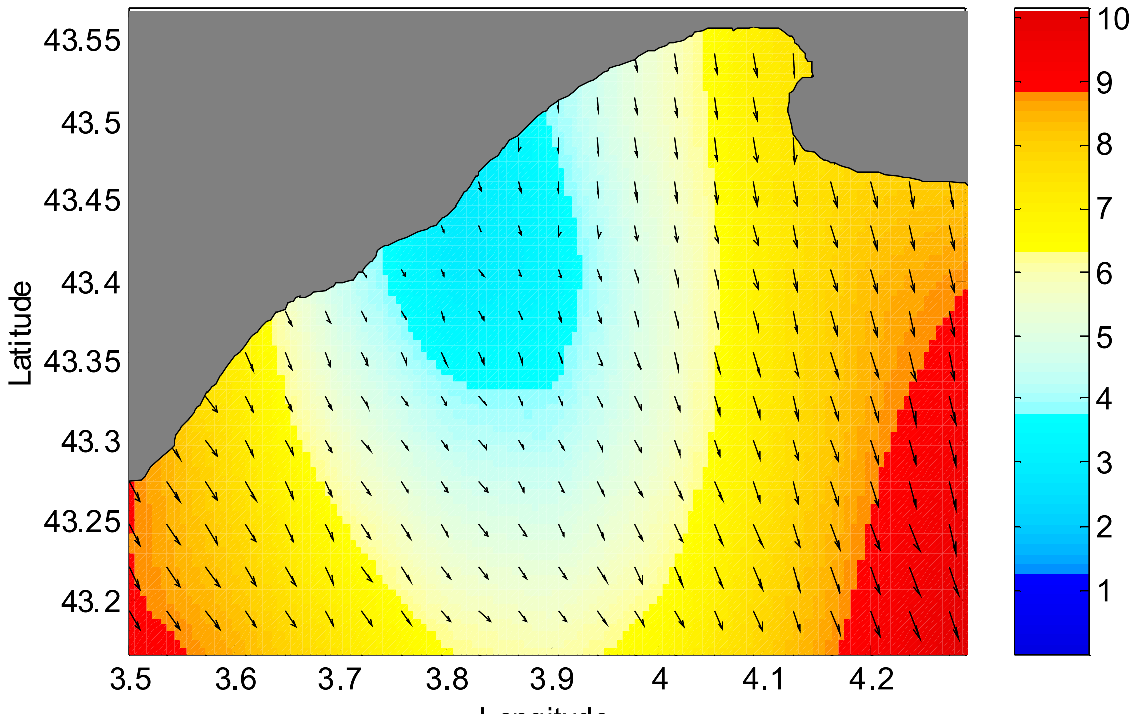

Fig. 5: Wind (arrows and colors ; m s^{-1}) modeled by Aladin at 12h00 on March 6.

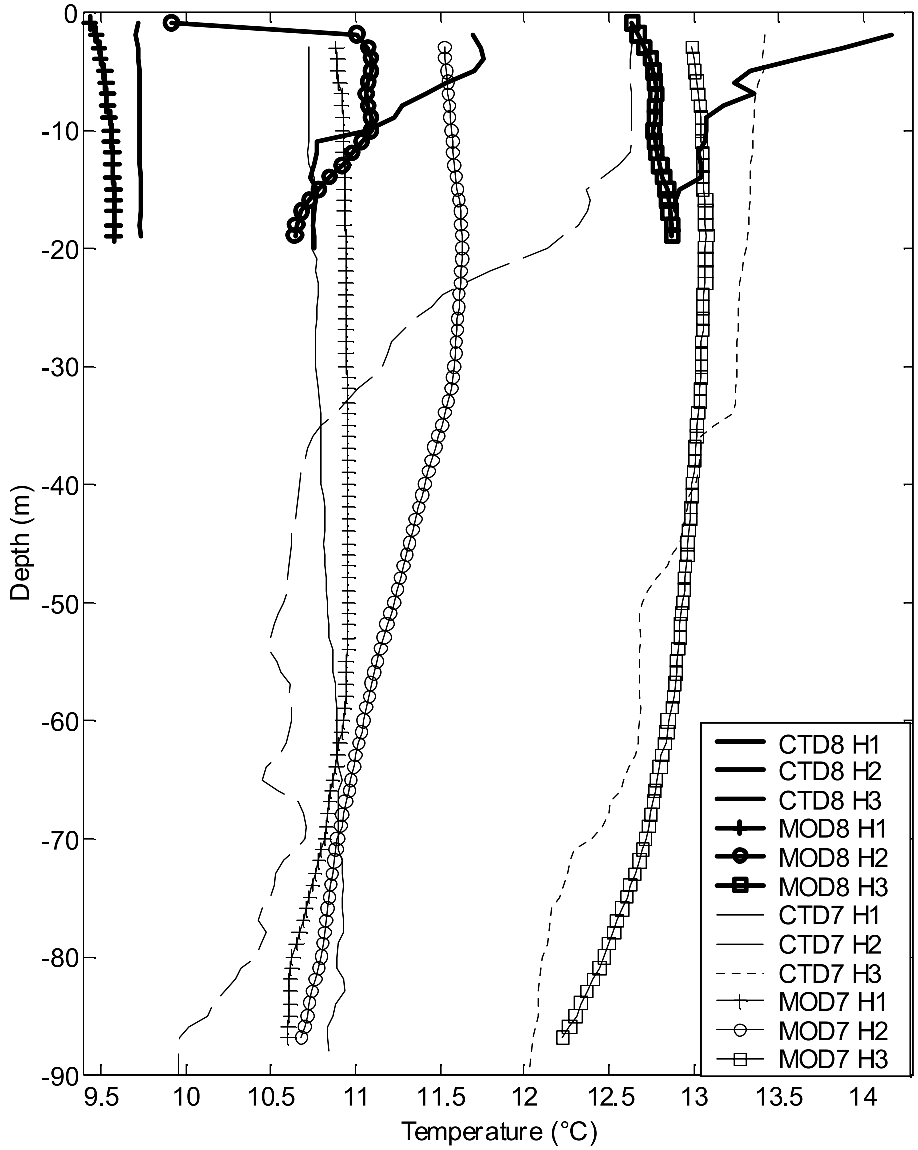

Fig. 6: Temperature profiles :

- measured at station 8 during HYGAM 1, at 18h10 on March 6 (CTD8 H1), during HYGAM 2, at 6h33 on March 20 (CTD8 H2), during HYGAM3, at 20h11 on April 5 (CTD8 H3),
- simulated at the same place and times (MOD8 H1, MOD8 H2, MOD8 H3) ,
- measured at station 7 during HYGAM 1, at 11h04 on March 6 (CTD7 H1), during HYGAM 2, at 0h16 on March 21 (CTD7 H2), during HYGAM3, at 8h50 on April 5 (CTD7 H3),
- simulated at the same place and times (MOD7 H1, MOD7 H2, MOD7 H3) .

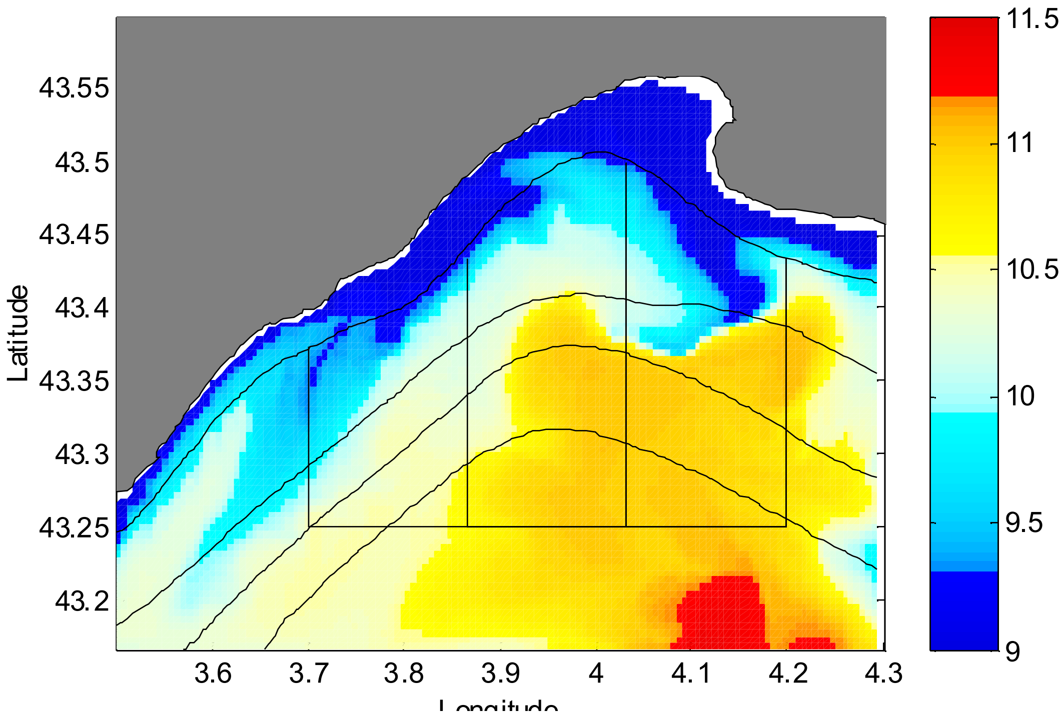

Fig. 7a: Surface temperature (°C) modeled by Symphonie at 12h00 on March 6.

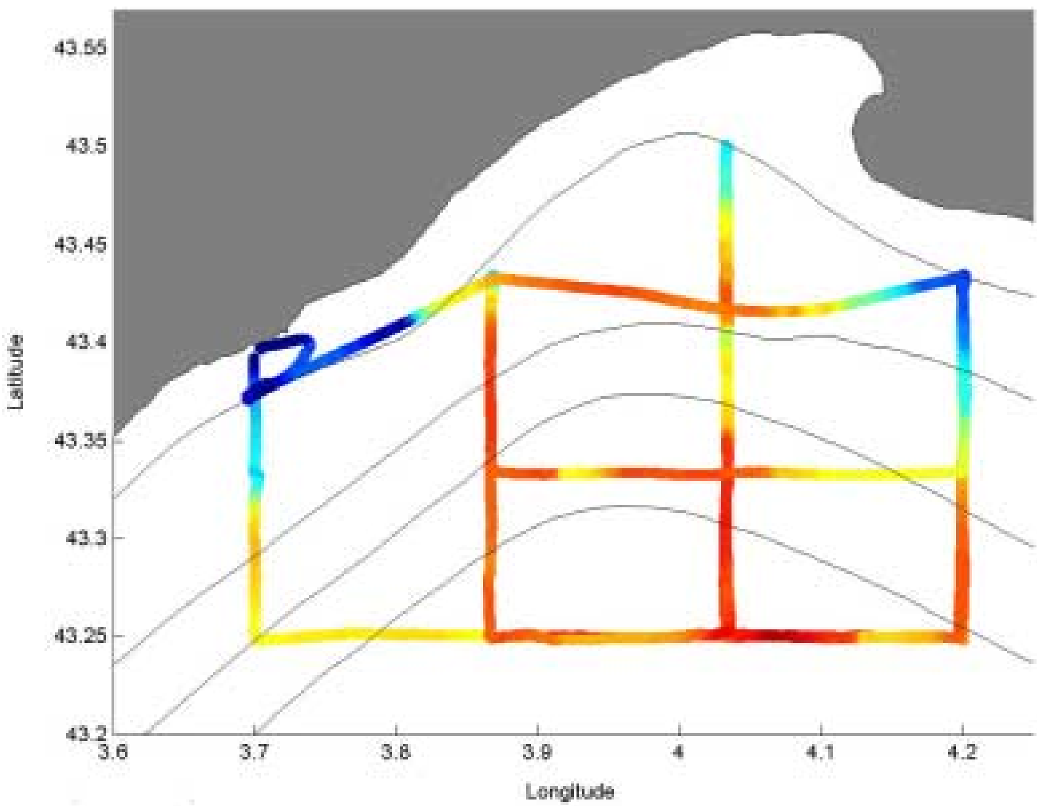

Fig. 7b: Surface temperature (°C) measured by the Téthys' thermosalinograph on March 6 (same color scale than Fig. 7a)

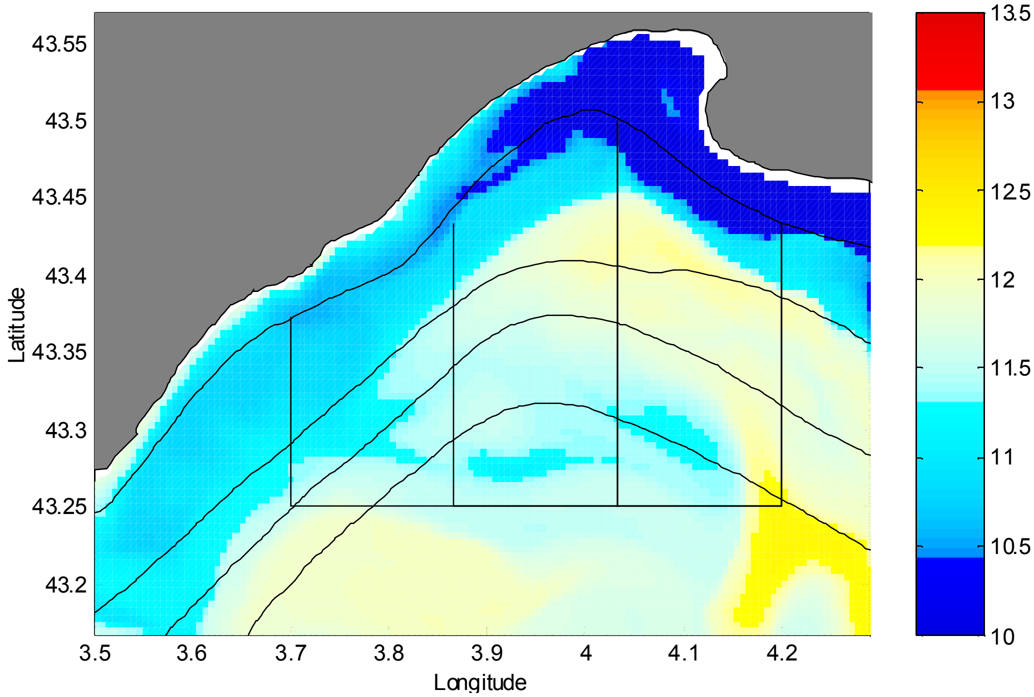

Fig. 7c: Surface temperature (°C) modeled by Symphonie at 12h00 on March 20.

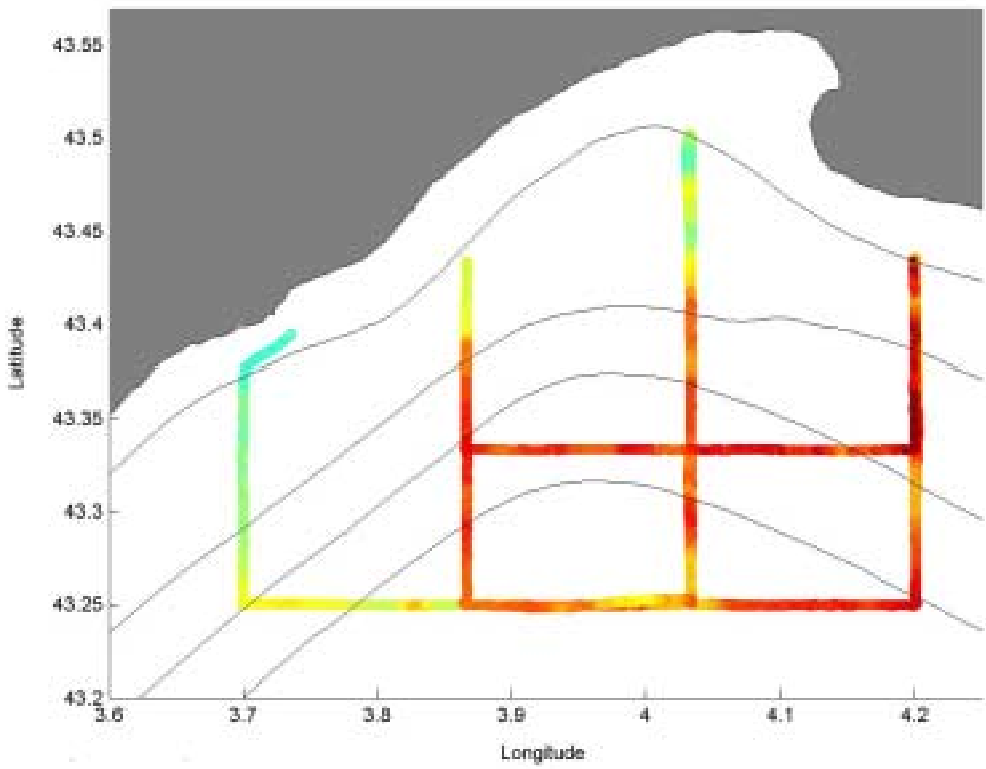

Fig. 7d: Surface temperature (°C) measured by the Téthys' thermosalinograph on March 20 (same color scale than Fig. 7c)

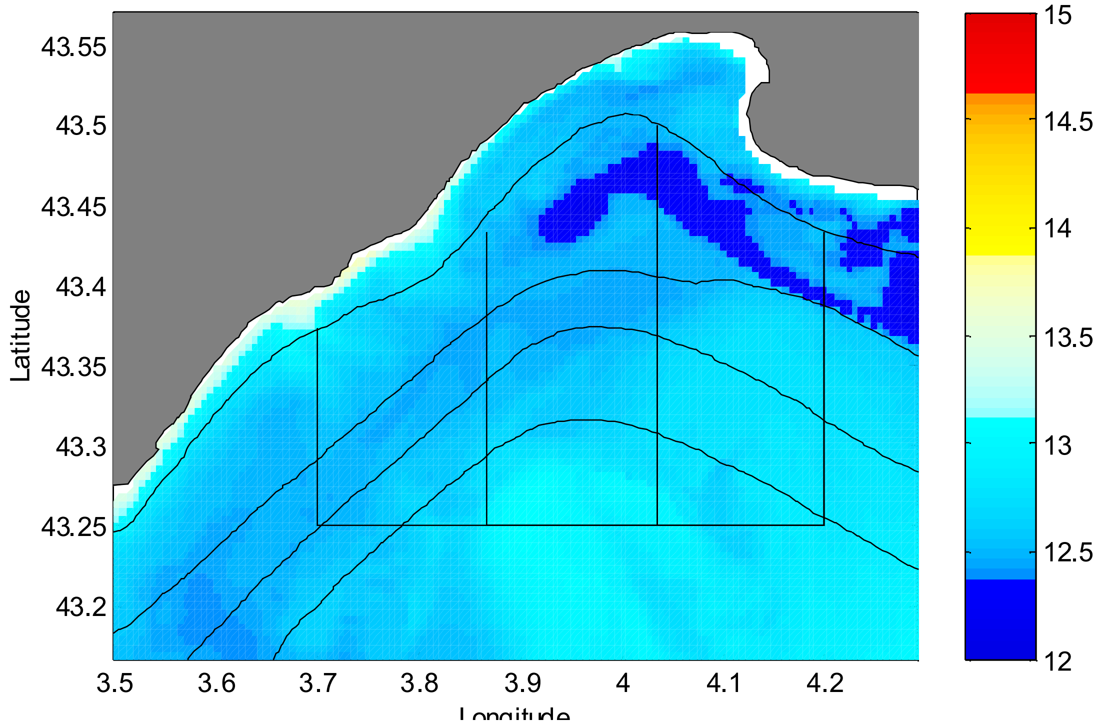

Fig. 7e: Surface temperature (°C) modeled by Symphonie at 21h00 on April 5.

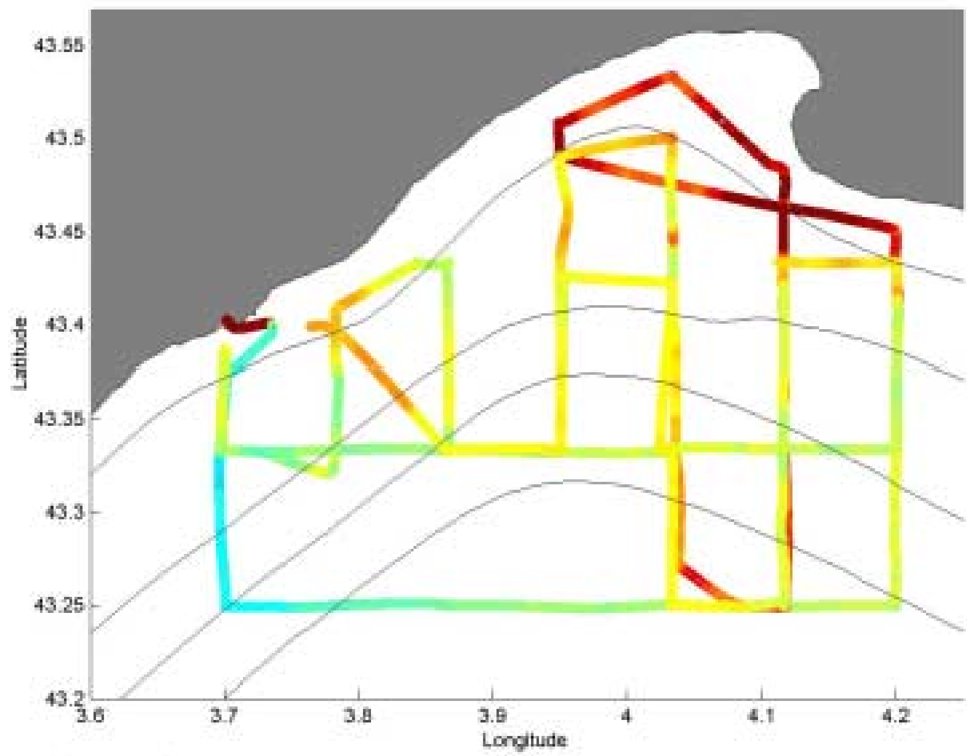

Fig. 7f: Surface temperature (°C) measured by the Téthys' thermosalinograph on April 5
(same color scale than Fig. 7e)

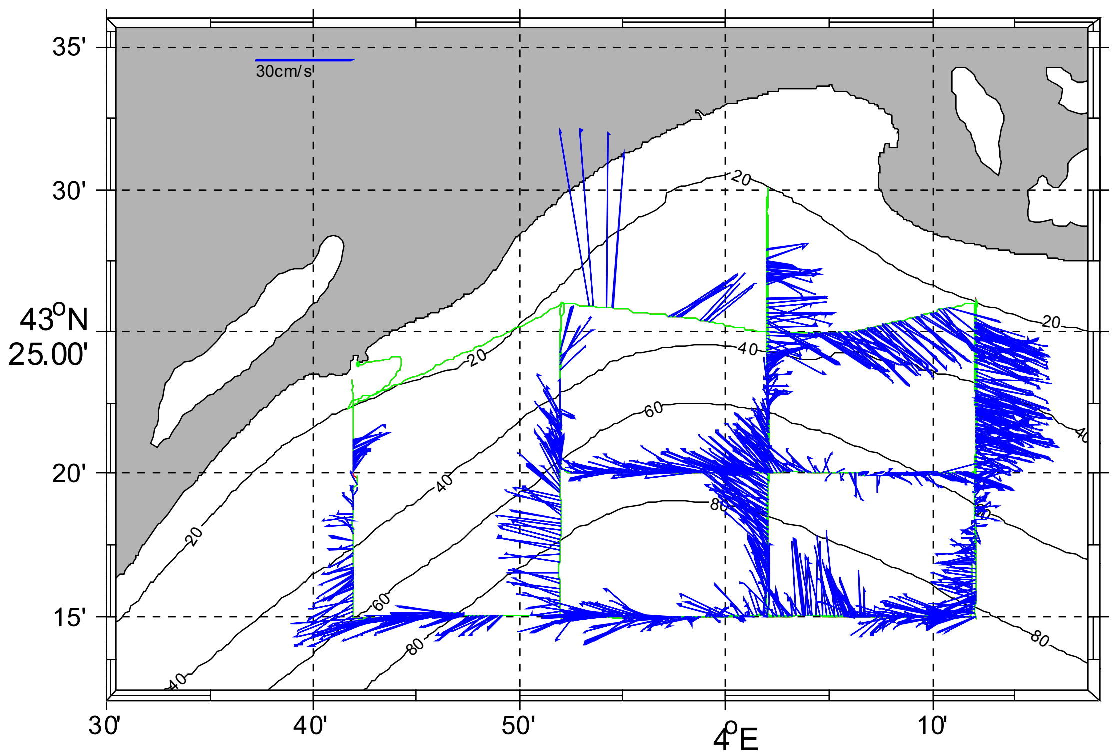

Fig. 8: Currents measured at 16 m depth along the cruise track between 8h00 on March 6 and 6h00 on March 7.

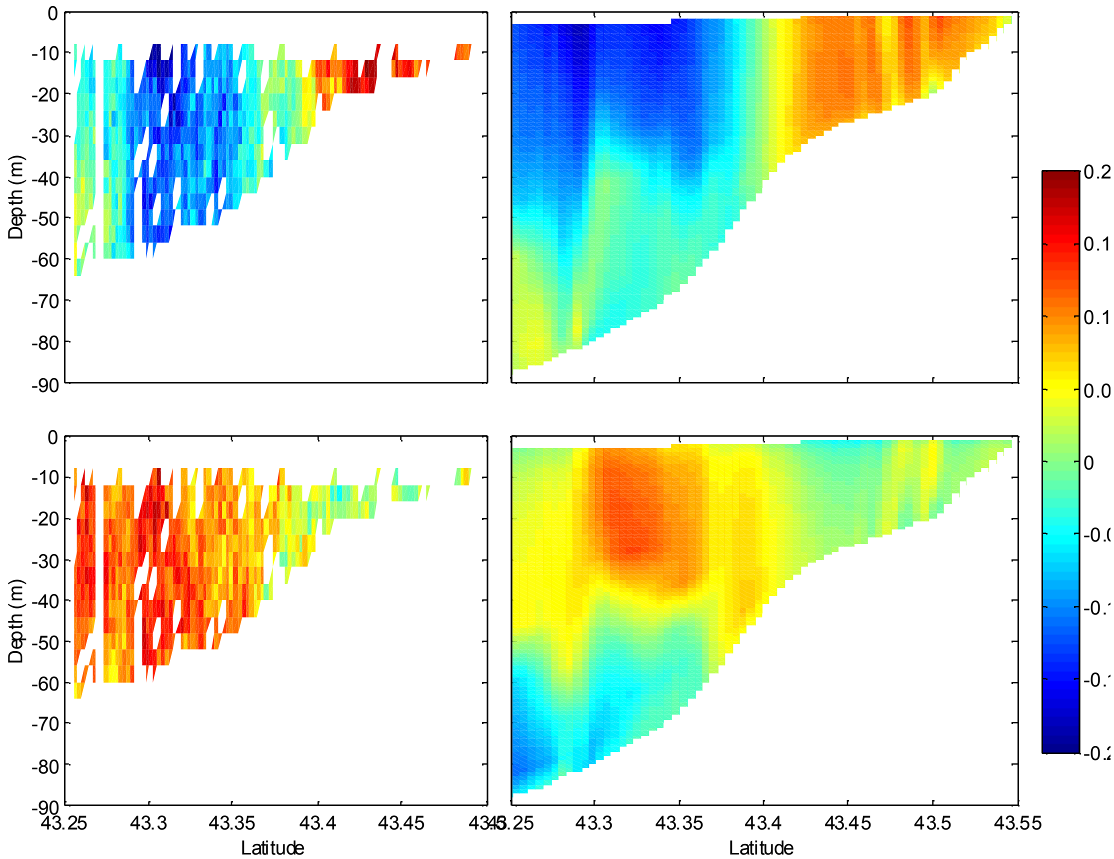

Fig. 9: Vertical sections (depth vs. latitude) of the currents (colors, m s^{-1}) on March 6 along transect 8-7 (longitude 4°02'E): (a) observed eastward component, (b) simulated eastward component, (c) observed nothward component, (d) simulated northward component

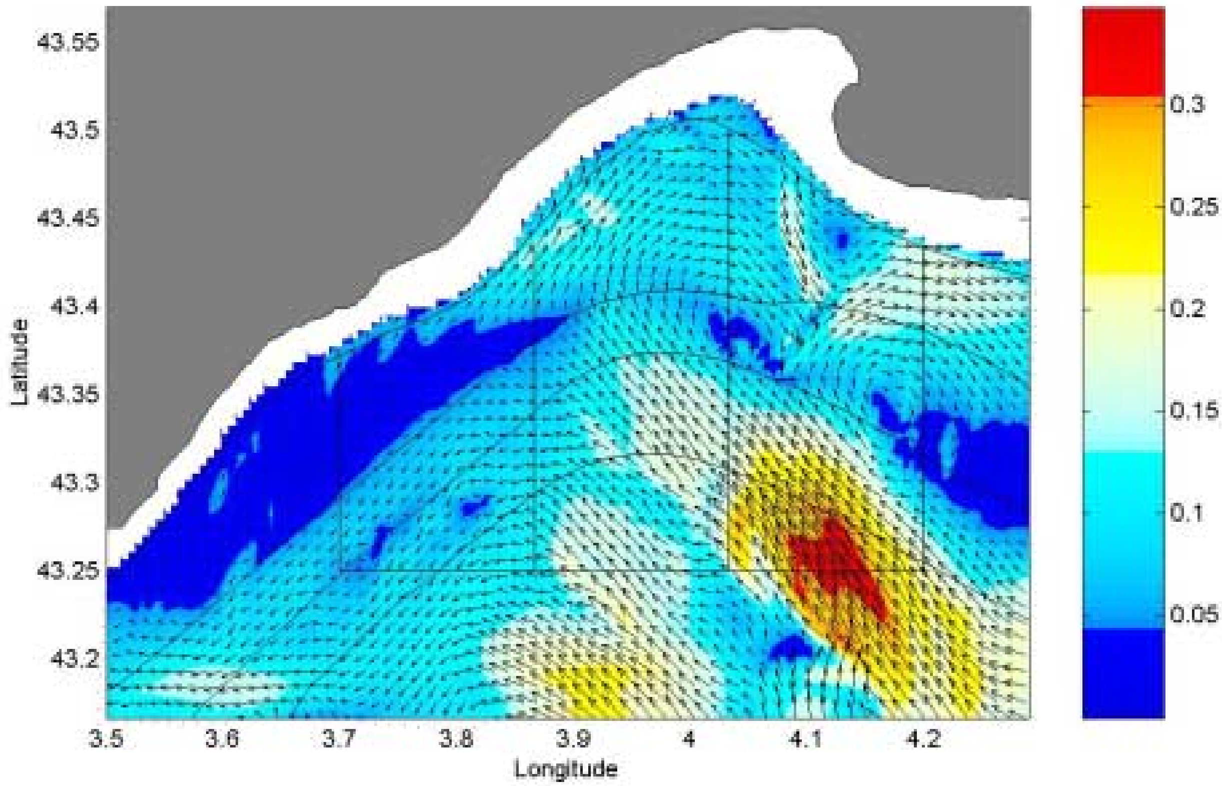

Fig. 10: Currents (colors, m s^{-1}) modeled by Symphonie at 12h00 on March 6 at 16 m depth

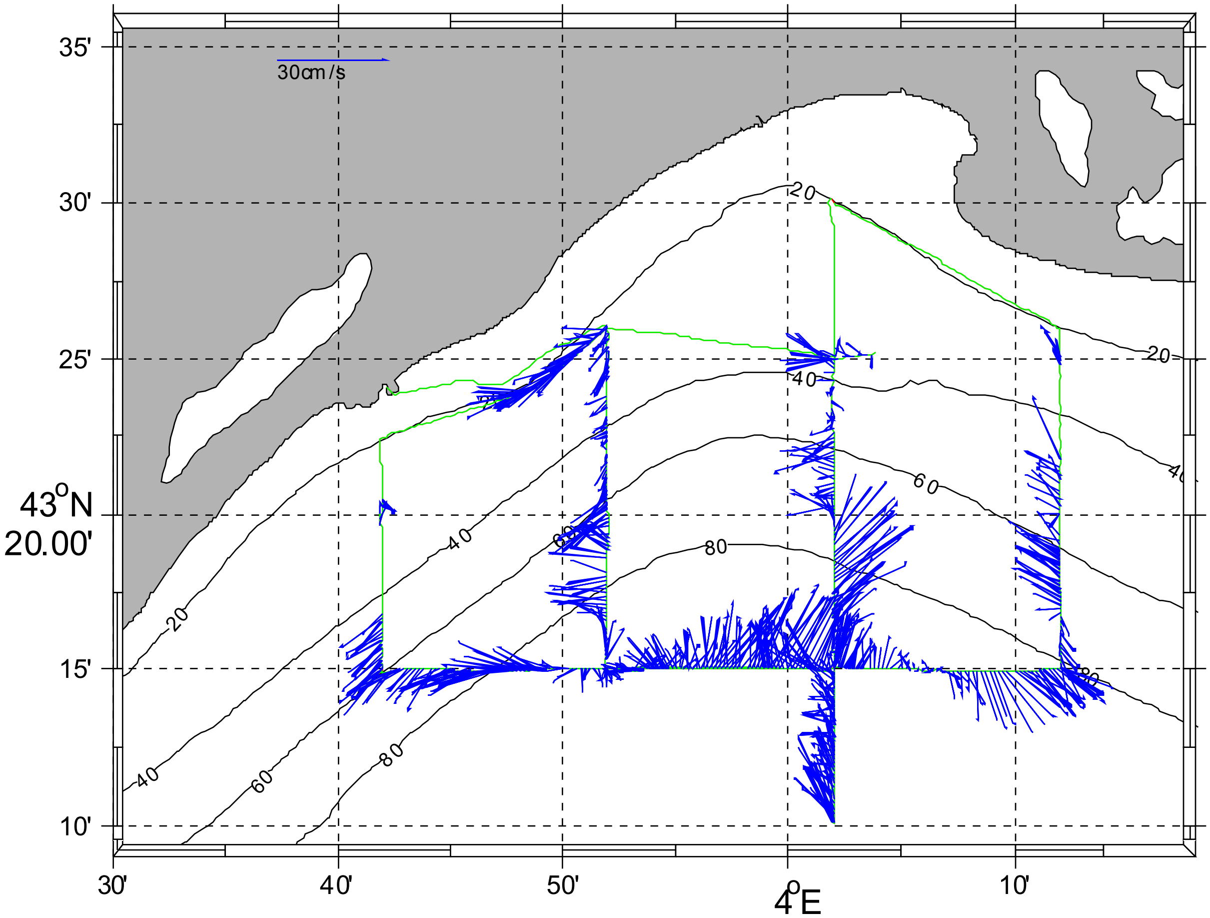

Fig. 11: Currents measured at 12 m depth along the cruise track beetween 17h00 on March 20 and 15h00 on March 21

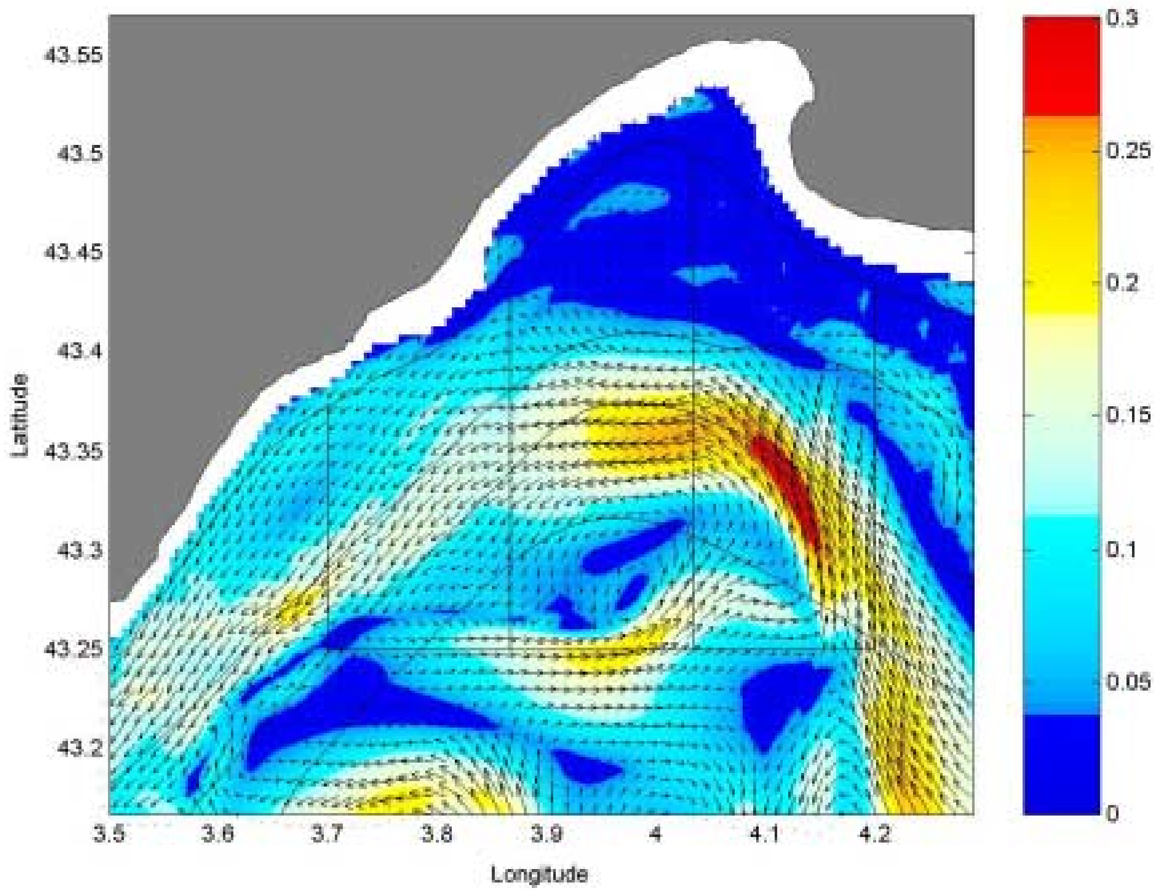

Fig. 12: Currents (colors, m s^{-1}) modeled by Symphonie at 06h00 on March 21 at 16 m depth.

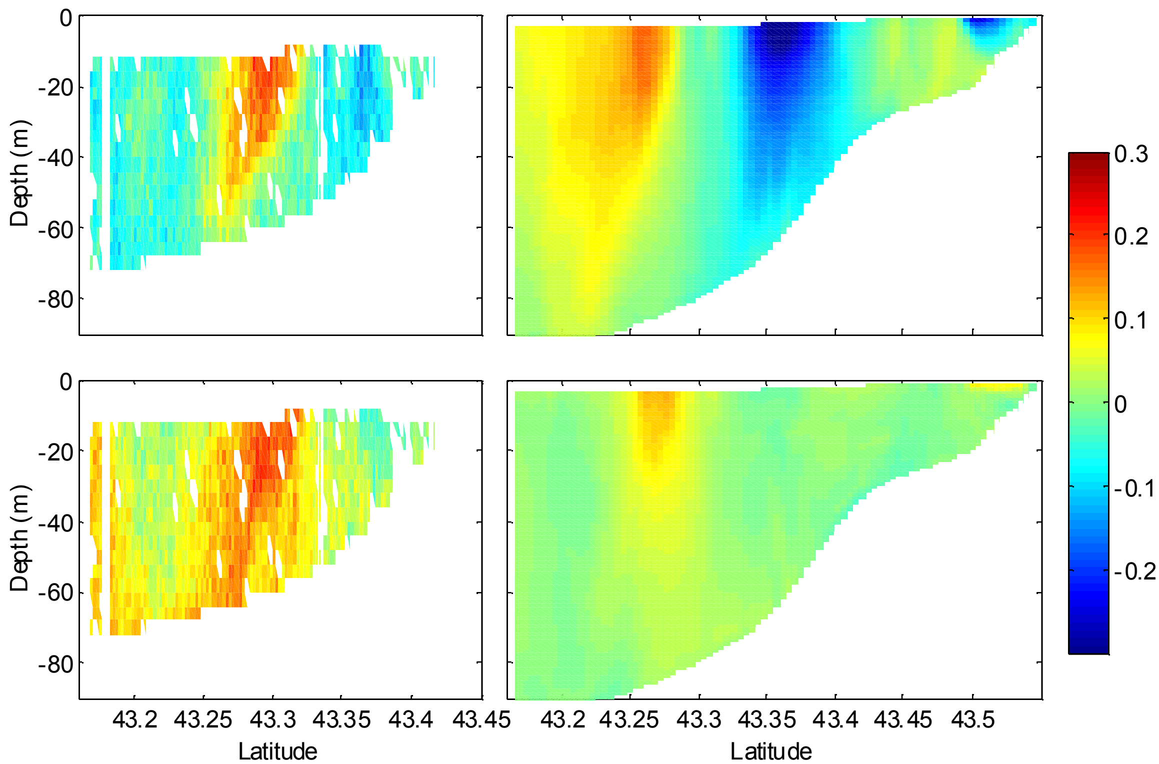

Fig. 13 : Vertical sections (depth vs. latitude) of the currents (colors, m s^{-1}) on March 21 along transect 8-7 (longitude 4°02'E): (a) observed eastward component, (b) simulated eastward component, (c) observed nothward component, (d) simulated northward component

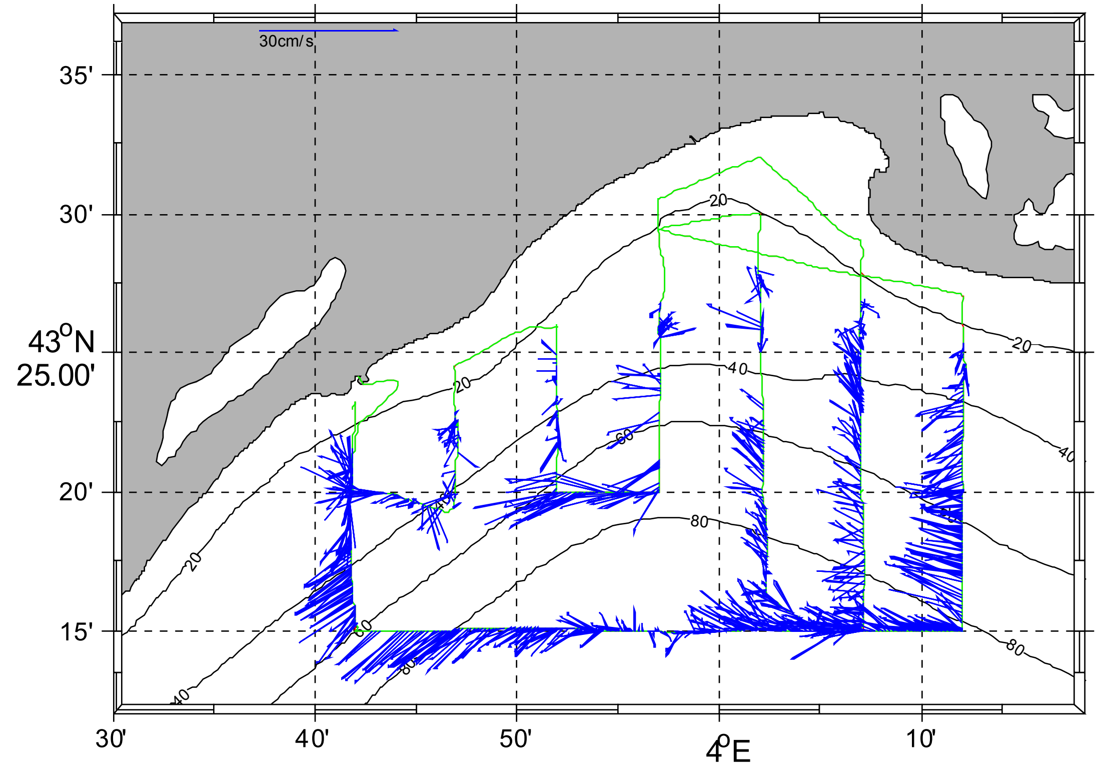

Fig. 14: Currents measured at 16 m depth along the cruise track beetween 6h00 on April 5 and 5h00 on April 6

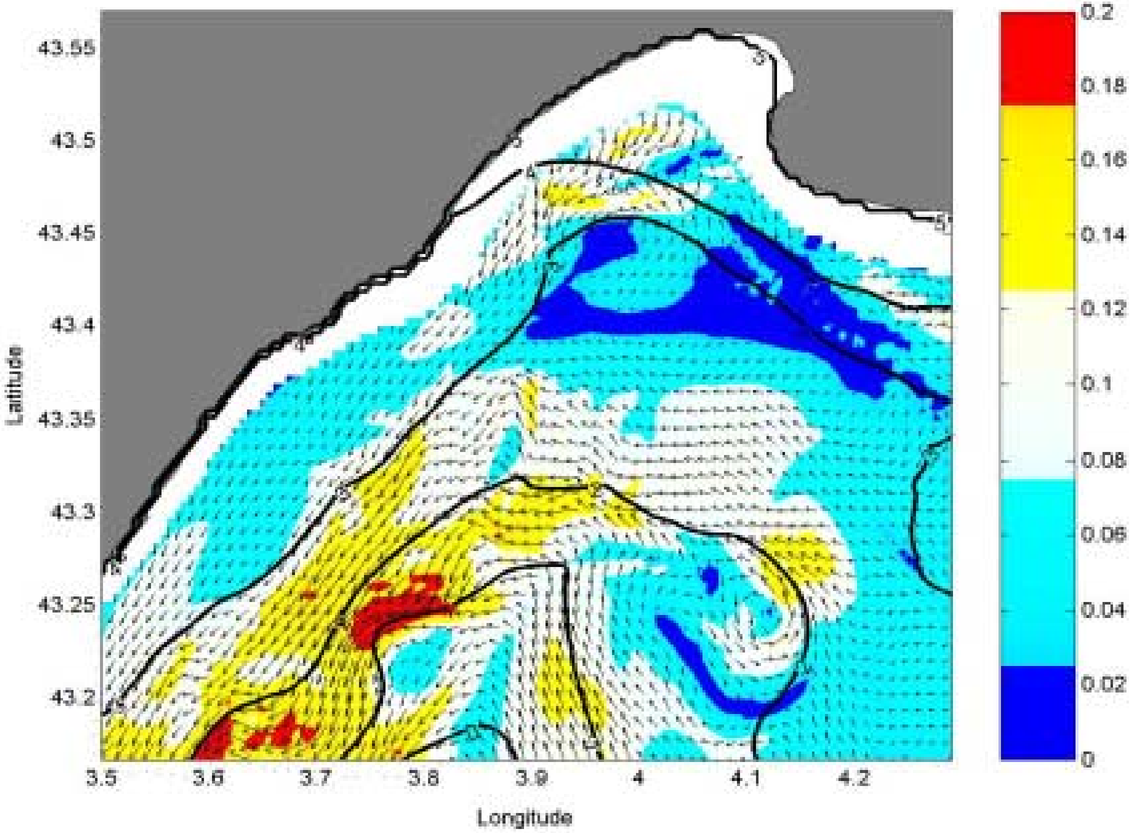

Fig. 15: Currents (colors and arrows, m s^{-1}) and surface elevation (black isolines, cm) modeled by Symphonie at 12h00 on April 5 at 16 m depth

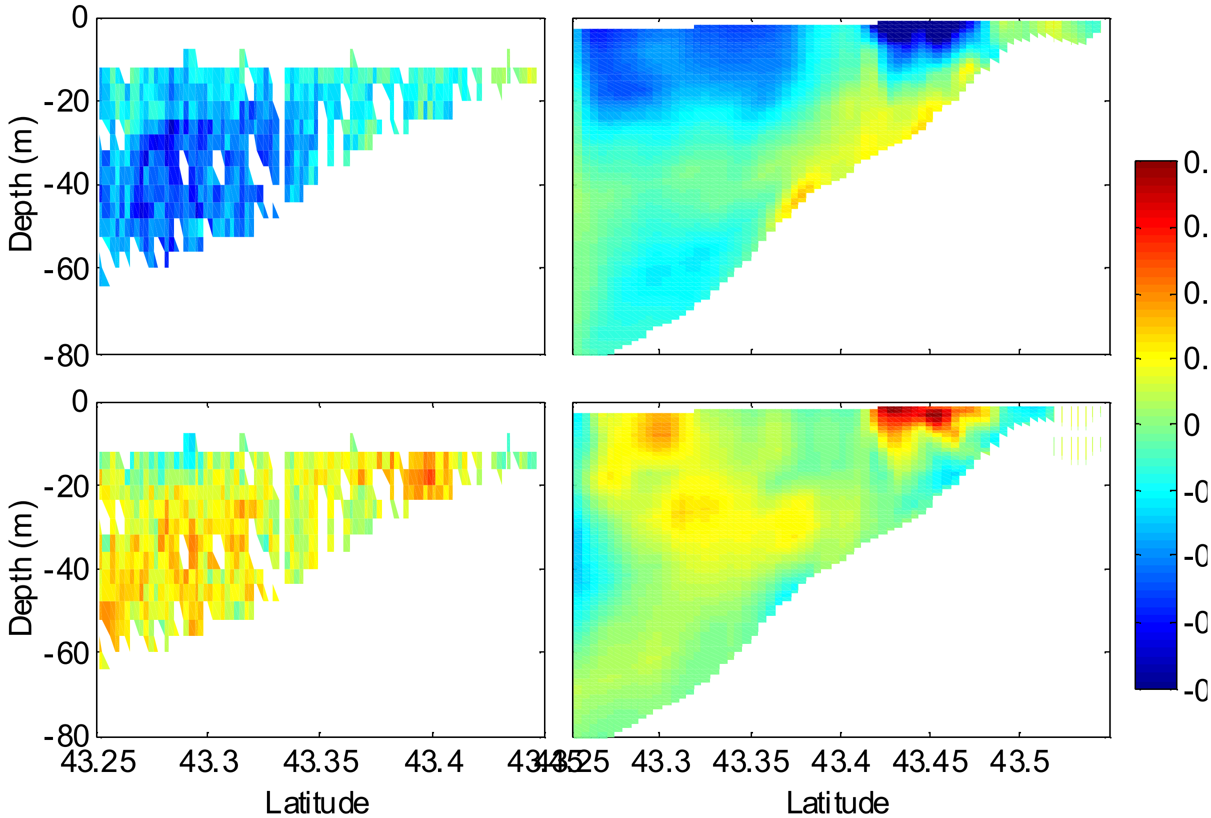

Fig. 16 : Vertical sections (depth vs. latitude) of the currents (colors, m s^{-1}) on April 5 along transect 8-7 (longitude 4°02'E): (a) observed eastward component, (b) simulated eastward component, (c) observed nothward component, (d) simulated northward component

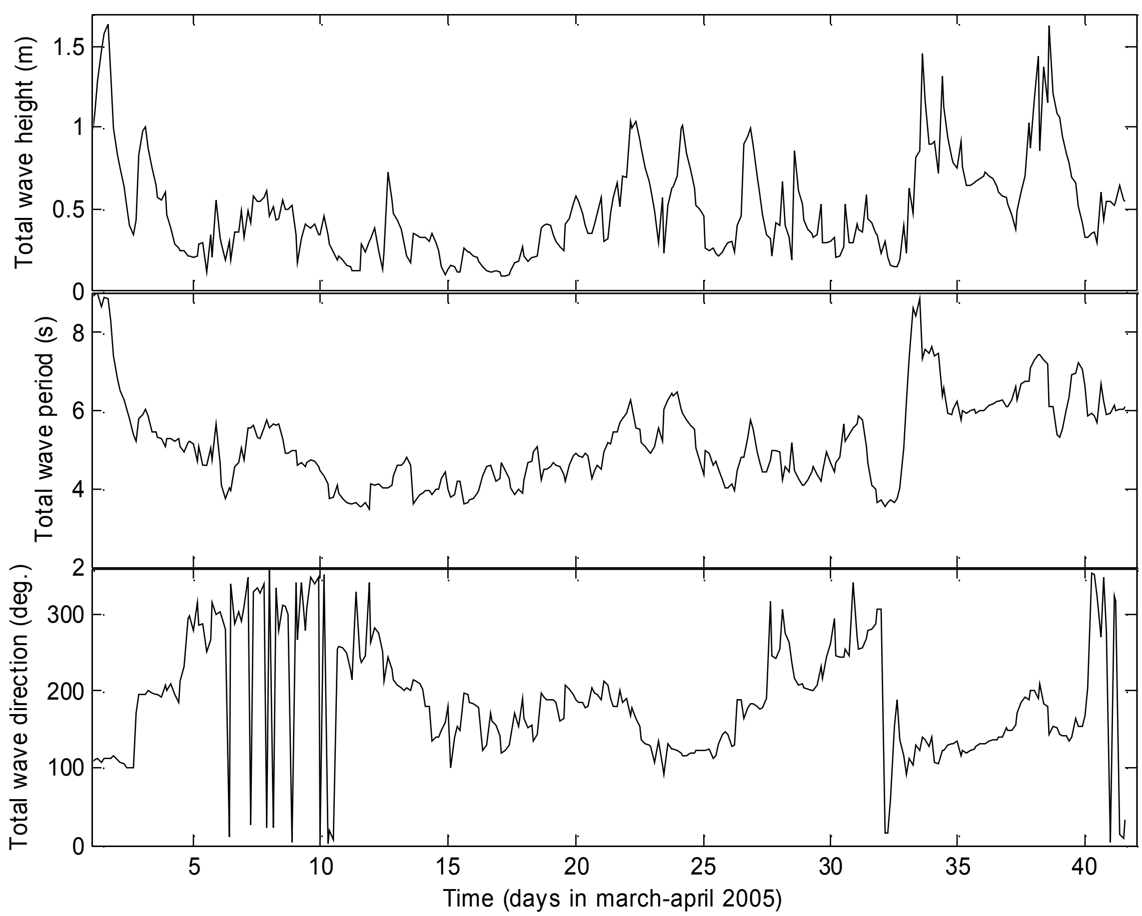

Fig. 17 : Total wave characteristics simulated by Vagmed Météo-France model at 43.25°N, 4.00°E